Georgia State University
Digital Archive @ GSU

Geosciences Theses | Department of Geosciences

12-2-2011

Whole-Rock Lead-Lead Systematics and Major Element Analyses on the 1.85 GA. FLIN FLON Paleosol, Manitoba, Canada: Implications for Uranium Mobility.

Federico Arturo Valencia
Federico Arturo Valencia Diaz, federicovalencia1@gmail.com

Follow this and additional works at: http://digitalarchive.gsu.edu/geosciences_theses

Recommended Citation
Valencia, Federico Arturo, "Whole-Rock Lead-Lead Systematics and Major Element Analyses on the 1.85 GA. FLIN FLON Paleosol, Manitoba, Canada: Implications for Uranium Mobility." (2011). *Geosciences Theses*. Paper 40.

This Thesis is brought to you for free and open access by the Department of Geosciences at Digital Archive @ GSU. It has been accepted for inclusion in Geosciences Theses by an authorized administrator of Digital Archive @ GSU. For more information, please contact digitalarchive@gsu.edu.

WHOLE-ROCK LEAD-LEAD SYSTEMATICS AND MAJOR ELEMENT ANALYSES ON THE 1.85 GA. FLIN FLON PALEOSOL, MANITOBA, CANADA: IMPLICATIONS FOR URANIUM MOBILITY.

by

FEDERICO A. VALENCIA

Under the Co-direction of Drs. Eirik J. Krogstad and W. Crawford Elliott

ABSTRACT

The 1.85 Ga Flin Flon paleosol located in Flin Flon, Manitoba, Canada, is studied with the purpose of determining the timing and geochemical trend of uranium migration. Radiometric minimum ages of sediments and paleosols indicates the presence of a post-depositional event, these ages are bracketed by the Trans-Hudson orogeny event (2155–1750 Ma) which resulted in the alteration of κ(Th/U) and μ(U/Pb) ratios by exposing volcanics to the atmosphere and instigating the mobilization of U. The profile shows that the Missi sediments lost Uby 84% average relative to corrected average upper crust value. The upper paleosol gained U by 11% and the lower paleosol lost U by 17%, relative to least weathered parent volcanics. Upward addition of U within the paleosol is associated with metasomatism. Potential mineralization of uranium occurs downgradient of the Missi and paleosol contact.

INDEX WORDS: Flin Flon paleosol, Missi Formation, Pb isotopes, Th/U, U/Pb, Time-integrated, Index of alteration.

WHOLE-ROCK LEAD-LEAD SYSTEMATICS AND MAJOR ELEMENT ANALYSES ON THE 1.85 GA. FLIN FLON PALEOSOL, MANITOBA, CANADA: IMPLICATIONS FOR URANIUM MOBILITY.

by

FEDERICO A. VALENCIA

A Thesis Submitted in Partial Fulfillment of the Requirements for the Degree of

Master of Science

In the College of Arts and Sciences

Georgia State University

2011

Copyright by

Federico Arturo Valencia

2011

WHOLE-ROCK LEAD-LEAD SYSTEMATICS AND MAJOR ELEMENT ANALYSES ON THE 1.85 GA. FLIN FLON PALEOSOL, MANITOBA, CANADA: IMPLICATIONS FOR URANIUM MOBILITY.

by

FEDERICO A. VALENCIA

Committee Chair: Dr. W. Crawford Elliott

Committee: Dr. Daniel M. Deocampo

Dr. Jeremy Diem

Electronic Version Approved:

Office of Graduate Studies

College of Arts and Sciences

Georgia State University

December 2011

DEDICATION

The present work is dedicated to my family, especially to my father in heaven whose lively encouragement and support is and will always be essential in my life.

ACKNOWLEDGEMENTS

Thanks Dr. Krogstad for kindly taking the time in the necessary laboratory training for Pb-Pb systematics, invaluable advice in the starting process, and friendship. Thanks to Dr. Deocampo's insightful comments and advice with the XRF analyses; and Dr. Crawford Elliott, for his time in the revision of this thesis and his service as the department chair. I would like to thank Kelly Gilmore, Hudson Bay Minerals and Dr. Andrey Bekker for providing me with the samples used in this thesis. Thanks to Dr. Jeremy Diem for your willingness to serve graduate students. Also, thanks to the geoscience department for their encouragement and financial support in the form of teaching assistantship; Ms. Basirat Lawal's administrative help and MS Atieh Tajik Lab assistance is greatly appreciated. Thanks to MS Alyssa Wright for her valuable help in the editing and formatting process. Finally, thanks to the graduate students whose company and friendship made me feel at home and to great friends/family outside the department.

TABLE OF CONTENTS

ACKNOWLEDGEMENTS v

LIST OF TABLES viii

LIST OF FIGURES ix

ABBREVIATIONS x

1. INTRODUCTION 1

2. BACKGROUND 3

Lead-Lead Systematics 3

Major Element Geochemistry 4

3. GEOLOGIC SETTING 6

4. ANALYTICAL METHODS 9

Whole-Rock Lead-Lead Isotope Analysis 9

Major Element Analysis 11

5. RESULTS 13

Whole-Rock Lead-Lead Isotope Analysis 13

Major Element Analysis 16

6. DISCUSSION 38

7. CONCLUSIONS 44

REFERENCES 45

APPENDICES 49

APPENDIX 1: Pb Isotope Analytical Methodology 49

APPENDIX 2: XRF Analytical Methodology 52

APPENDIX 3: Error Estimates for ICPMS Measurements 54

APPENDIX 4: Error Estimates for XRF Measurements 55

LIST OF TABLES

Table 5.1 Measured whole-rock Pb isotopic composition, measured μ (U/Pb), time-integrated μ† (U/Pb) and κ† (Th/U) calculated required values for observed lead composition using age of 1906 Ma, κ (Th/U) average upper crustal ratio of 3.86 predicted by the Kramers and Tolstikhin (1997) for Pb isotope growth model; and ΔU, gain indicated by +, loss indicated by -.. 34

Table 5.2 Measured major element oxides (wt %) and trace element concentrations (ppm). 35

Table 5.3 Percentagegain/lossratio of major and trace elements from altered samples relative to least altered sample 37

LIST OF FIGURES

Figure 3.1 Location of drill core, and galena (Thorpe, 2008) 8

Figure 5.1 $^{206}Pb/^{204}Pb$ vs. $^{207}Pb/^{204}Pb$ whole-rock isotope ratio diagram for volcanic samples.. 22

Figure 5.2 $\kappa^{\dagger}$ (Th/U) vs. depth 23

Figure 5.3 $\kappa^{\dagger}$ (Th/U) vs. $1/\mu^{\dagger}$ (Pb/U) 24

Figure 5.4 1/μ (U/Pb) vs. CIA for paleosols... 24

Figure 5.5 $^{206}Pb/^{204}Pb$ vs. $^{207}Pb/^{204}Pb$ whole-rock isotope ratio diagram for paleosols 25

Figure 5.6 $^{206}Pb/^{204}Pb$ vs. $^{207}Pb/^{204}Pb$ whole-rock isotope ratio diagram for sediments... 25

Figure 5.7 $^{206}Pb/^{204}Pb$ vs. $^{208}Pb/^{204}Pb$ whole-rock isotope ratio diagram..... 26

Figure 5.8 $^{238}U/^{204}Pb$ vs. $^{206}Pb/^{204}Pb$ whole-rock Isochron for paleosols and sediments..... 27

Figure 5.9 AFM diagram for volcanics of the Flin Flon area... 28

Figure 5.10 Stratigraphic section and profile geochemical variations... 29

Figure 5.11 CIA and PIA vs. depth. 30

Figure 5.12 Percentage change (gain/loss) ratios (normalized to TiO_2) as a function of weathering intensity (CIA index)..... 31

Figure 5.13 A-CN-K diagram (molecular proportions) 33

Figure 5.14 (Al_2O_3-K_2O)-CaO*-NaO diagram (molecular proportions). 33

Figure 6.1 Measured uranium concentration (ppm) vs. depth... 43

ABBREVIATIONS

μ: Th/U ratio

κ: U/Pb ratio

$\kappa^{\dagger}$: Time-integrated Th/U

$\mu^{\dagger}$: Time-integrated U/Pb

Pb: Lead

Ca: Calcium

Na: Sodium

K: Potassium

U: Uranium

Th: Thorium

CIA: Chemical Index of Alteration

PIA: Plagioclase Index of Alteration

MSWD: Mean square weighted deviation

1 INTRODUCTION

Paleosols are formed through interactions of the hydrosphere, atmosphere, and biosphere on rocks. The ~1.85 Ga Flin Flon paleosol located in Flin Flon, Manitoba, Canada, was developed on the greenschist-grade metamorphosed Amisk mafic volcanics. Holland et al., (1989) showed evidence of increasing oxygen content in the atmosphere and consequent oxidative weathering during the middle Proterozoic. Oxidizing conditions are capable of altering the oxidation state of redox-sensitive elements such as U, Fe, Cr, and Mo, resulting in the differential mobility of various elements in a rock. Under oxidative weathering, the Th/U (κ) elemental ratio of the parent rock increases while the U/Pb (μ) ratio decreases because of the dissimilar redox behavior of Th, Pb, and U (McLennan and Taylor, 1980; Krogstad, 2004). Therefore, oxidative weathering losses of U from a parent rock causes fractionation of Th/U and Pb/U elemental ratios.

In the study of elemental mobility (gain or loss) of U from a parent rock, careful consideration should be taken in the determination of the least altered rock or parent rock, especially when petrographic and field relationships are limited. One problem rests in the direct measurements of Th/U or U/Pb ratios of parent rocks, which are often misleading because of the post-depositional uranium mobility (Pollack et al, 2009). Nevertheless, U and Th radioactively decay to radiogenic Pb isotopes at known rates, thus measurement of Pb isotope composition are useful to calculate the time-integrated Th/U and U/Pb depositional ratio of parent rocks (Rosholt et al, 1973; Pollack et al, 2009). If calculated time-integrated ratios are the same as observed ratios in the parent rock, then that rock is considered unaltered; otherwise alteration has occurred in the rock. Another problem in the determination of the extent of U mobility from a parent rock is the direct comparison between the amount of U required to produce the observed radiogenic

lead composition and the amount of U present in the rock (i.e., Rosholt and Bartel, 1969; Rosholt et al, 1973). Relative elemental gain or loss from a parent rock should consider volumetric, density, and geochemical changes in rock alteration (Gresens, 1967). Thus, in the determination of U gain or loss, the assumption of constant volume, density or immobile element should be considered prior to the determination of the extent of U mobility relative to an unaltered rock.

The purpose of this study is to determine the timing and trend of uranium migration after deposition of parent rocks. The objective is to delineate radiogenic lead isotopes in altered rocks that are not supported by observed uranium concentration in their parent by measuringlead isotopic compositionand the concentration of lead and uranium in whole rocks found in a drill core extracted from the Flin Flon area.

Comparison of geochemical trends between parent and altered rockwill contribute to the identification of potential pathways of fluids, pointing towards storage rocks that can potentially mineralize uranium over geological time processes.

Research Questions

- During the Flin Flon paleosol development, where could uranium be stored/accumulated?
- How much uranium is mobilized relative to the parent rock?

Purpose

- To determine the timing and geochemical trend of uranium migration.

Objectives

- Determine whole rock lead isotope ratios in altered rocks that are not supported by observed uranium concentration, and timing of alteration.
- Extent of U migration between altered and unaltered rocks

2 BACKGROUND

Lead-Lead Systematics

Uranium is a redox sensitive element having two common oxidation states (+4 and +6). Under oxic conditions,U^{+4} is oxidized to U^{+6}, and it is easily mobilized because of its high stability as uranyl phosphate ionic complexes at pH 4-7.5 and as carbonate ionic complexes at greater pH in oxygenated aqueous solutions (Langmuir, 1978). Thorium has only one oxidation state (+4) and is geochemically similar to U^{+4}; both are insoluble under surface conditions. Lead is largely immobile and is known to be removed from rocks mainly by chlorine rich brines (Doe et al., 1983; Sicree and Barnes, 1996). In general, U loss occurs as $U^{6+}$when rocks are exposed to oxidative weathering, therefore κ and μ values from the parent rock are altered under oxidative weathering.

Direct measurement of Th/U (κ) and U/Pb (μ) ratios and dating rest on the tenuous assumption that samples remained closed to U, Th, Pb, and intermediate daughters (Faure and Mensing, 2005). The use of long lived isotopes (^{232}Th and ^{238}U) and measurement of the accumulation of their respective radiogenic Pb isotopes (^{208}Pb and ^{206}Pb) allows for the calculation of the Time-integrated Th/U ratio ($\kappa^{\dagger}$) (Pollack et al., 2009)

$\kappa^{\dagger} = \frac{\lambda^{238}\mathrm{U}}{\lambda^{232}\mathrm{Th}} \times \frac{(^{208}Pb/^{204}Pb)_m - (^{208}Pb/^{204}Pb)_i}{(^{206}Pb/^{204}Pb)_m - (^{206}Pb/^{204}Pb)_i}$, where *m* and *i* stand for measured and initial respectively, and λ stands for decay constant. In the same manner, Time-integrated U/Pb ratios ($\mu^{\dagger}$) are calculated by using the radioactive decay of ^{238}Uto^{206}Pb from (Faure and Mensing, 2005)

$\mu^{\dagger} = \frac{(^{206}Pb/^{204}Pb)_m - (^{206}Pb/^{204}Pb)_i}{(e^{\lambda 238U * t_0} - 1)}$, where t_o is the time elapsed since whole rock closure to metamorphism. Such approach is possible because ^{232}Th and ^{238}U are long lived radionuclides with abundances of 100% and 99.3%, respectively. ^{232}Th and ^{238}U decay to their radiogenic ^{208}Pb

and ^{206}Pb isotope daughters at known rates, respectively. ^{204}Pb is non-radiogenic and has a constant abundance.

The process of metamorphism causes changes on the isotopic composition of minerals, making them unsuitable for lead isotopic relationships in rocks. This problem can be overcome by analyzing whole-rock Pb isotopic composition because of isotopic homogenization of minerals within the rock as a result of redistribution caused by metamorphism. Rosholt et al. (1973) showed the usefulness of whole-rock lead-lead isotope systematics in age determination despite the mobility of uranium and lead from the rock and minerals exposed to chemical weathering.

Major Element Geochemistry

Chemical Index of Alteration (CIA), as defined by Nesbitt and Young (1984, 1979), and Plagioclase Index of Alteration (PIA) (Fedo et al., 1995) are calculated using molar proportions of major element oxides. CIA is interpreted as the measure of the extent of conversion of feldspars (which are abundant in the upper crust) to clays as a function of weathering intensity. CIA values range from 30 to 45 for unweathered basalt, 45 to 55 for granites and granodiorites, 75 for muscovite, 75 to 85 for smectites, and 85 to 100 for kaolinite and chlorite. PIA value of 100 indicates the transformation of virtually all plagioclase to kaolinite or gibbsite; an index of 50 indicates unweathered plagioclase. In this study, both CIA and PIA define the extent of weathering in the profile.

$$CIA=[Al_2O_3/(Al_2O_3+CaO^*+Na_2O+K_2O)] \, x \, 100$$

$$PIA=[(Al_2O_3 - K_2O)/ (Al_2O_3+ CaO^*+Na_2O - K_2O)] \, x \, 100$$

$$CaO^*=\text{mol } CaO - \text{mol } CO_{2(cc)} - (0.5 \, x \text{ mol } CO_2)_{(dol)} - [(10/3)\text{mol } P_2O_5]_{(ap)}$$

CaO* is the CaO in the silicate fraction only. Where cc=calcite, dol=dolomite, and ap=apatite.

Based on Gresens' (1967) composition-volume equation in metasomatic alteration, Grant (1986) proposed a graphical solution for gains and losses of elements in the profile from chemical analyses calling it the Isocon method. This method plots altered chemical composition against unaltered chemical composition; through consideration of immobile elements, (Ti, Al, Fe(III) or Th) one can define an isocon (a straight line through the origin of the diagram). Such diagram requires re-scaling of data for clarity in the diagram; such scaling however does not affect the slope of the isocon (Grant, 2005). Relative gains and losses of mobile elements are given by the displacement of data points from the reference isocon. The measure of gain or loss is given by the percentage change in concentration of an element relative to its concentration prior to alteration. If an element oxide is assumed immobile through the profile, asAl_2O_3, then we use this formulae $\frac{\Delta C_i}{C_i^0} = \left(\frac{C_{Al_2O_3}^0}{C_{Al_2O_3}^A}\right)\left(\frac{C_i^A}{C_i^0}\right) - 1$; if constant mass is assumed then $\frac{\Delta C_i}{C_i} = \left(\frac{C_i^A}{C_i^0}\right) - 1$; if constant volume is assumed, $\frac{\Delta C_i}{C_i} = \left(\frac{\rho^A}{\rho^0}\right)\left(\frac{C_i^A}{C_i^0}\right) - 1$; where *o*, *A*, *i*, and *C* indicates unaltered sample, altered sample, component, and concentration, respectively. TiO_2 is used as a normalizing element instead of Al_2O_3(see results chapter for discussion). In this study, isocon diagrams are not plotted because of the bulky amount of graphs needed to produce them; instead, data is evaluated as gains or losses in the profile compared with weathering intensity. Therefore, percentage changes of elemental oxides are plotted as a function of weathering intensity (CIA index).

3 GEOLOGIC SETTING

The Flin Flon domain is part of the Paleoproterozoic Trans-Hudson Orogen, consisting of: Amisk volcanics deposited between 1.92 Ga and 1.88 Ga, syntectonic granitoid plutons emplaced between 1.87 Ga and 1.84 Ga, and Missi Formation deposited between 1.85 Ga and 1.84 Ga (composed of sediment deposits unconformably overlying the Amisk Formation) (Lucas et al., 1996) (Figure3.1).The Amisk Group is an accretionary complex formed by amalgamation of intraoceanic crustal rocks deposited in an island arc environment (Lucas et al., 1996). It is composed mainly of volcanic and plutonic rocks such as Tholeiitic basalts and andesites, coarse pyroclastics, high alumina basalt, dacites, and rhyolites. Tholeiitic basalts and andesites account for 85% of volcanic rocks deposited in a marine environment and the remaining 15% is formed by dacite and rhyolite deposited in a subaerial environment (Holland et al., 1989). The Missi Group deposited in alluvial fan environments contains well rounded clasts of the Amisk group, reworked paleosols, clasts of granite, granitic gneiss, chert, jasper, and magnetite or hematite (Stauffer, 1990).

Below the Missi-Amisk contact, subaerial weathering of the Amisk Group gave rise to the formation of the Flin Flon paleosol. Rye and Holland (1998) consider this paleosol as a definite paleosol occurrence. Holland et al. (1989) observeda gradual and continuous change in texture, mineralogy, and chemical composition of the parent material towards the Missi-Amisk contact and affirmedthat the Flin Flon area has been subjected to greenschist-grade metamorphism associated with the Hudsonian Orogeny (~1.8 Ga), as evidenced by the presence of chlorite, actinolite, epidote, quartz, albite, calcite, magnetite and pyrite. However, such metamorphic alteration was not pervasive, since most of the samples seemed to retain much of their original igneous fabric. Pan and Stauffer (2000) gave a chemical age of 1.85-1.0 Ga for

uraninite grains in the paleosol and Missi sediments. Such age also correlates well with the emplacement of the Penokean orogeny at ~1.85 Ga (Schulz and Cannon, 2007).

Samples for this study belongs to the drill-core FS44, from Flin Flon, Manitoba, Canada, drilled at an angle of ~33° by the Hudson Bay Minerals Company. Drill-core contains regolith; sampling interval goes from 398 to 432 meters below surface. Below is the description of the drill-core provided by Dr. Andrey Bekker

Depth (m)	**Description**
404.0	Missi, pebbly sandstone with thin rare tuff layers;
405.0	Missi, Pebbly sandstone. Starts with thin (3-4 cm in thickness) silty layers (?tuffs). Contact seems to show some indication of structural complication such veins of quartz, minor displacement;
405.1	Oxidized pebbles of jasper eroded from the paleosol, oxidized pieces of paleosol in the lower part of the Missi continue up to 398.0 m;
406.2	Red-colored (oxidized) upper part of the paleosol. Corestones have outer rim oxidized;
406.4*	Oxidized (red) layer in the paleosol;
407.2	Minor admixture of detrital quartz grains into the paleosol. Their abundance increase upsection;
408.4	Altered corestones of basalt in paleosol; also, at 409.6 m – 15cm in thickness, another layer with corestones at 409.4 m. 408.4 C= corestone, 408.4 P=paleosol;
409.2	Paleosol starts;
~410.0	There is the contact with the paleosol, but zones of fractures (?vertical dikes) start to appear at 410.2-410.25 m. These dikes make irregular contact with the paleosol;
410.23	Altered basalt and thin layer of paleosol (5 cm);
414.36 i	Layer of intrusion;
414.36 v	Volcanics;
424.0	Starts bleached and episotized basalt;
425.95	Massive fine-grained basalt with cubic pyrite in veins. Pyrite has black halos of chlorite. Some volcaniclastics with porphyritic basalt are epidotized. Epidotization and bleaching of basalt and volcaniclastics increases upsection with cubes of pyrite up to 1 cm in size developed;
431.4	Fine grained basalt passing to altered veined basalt with quartz, pyrite, and jasper veins.

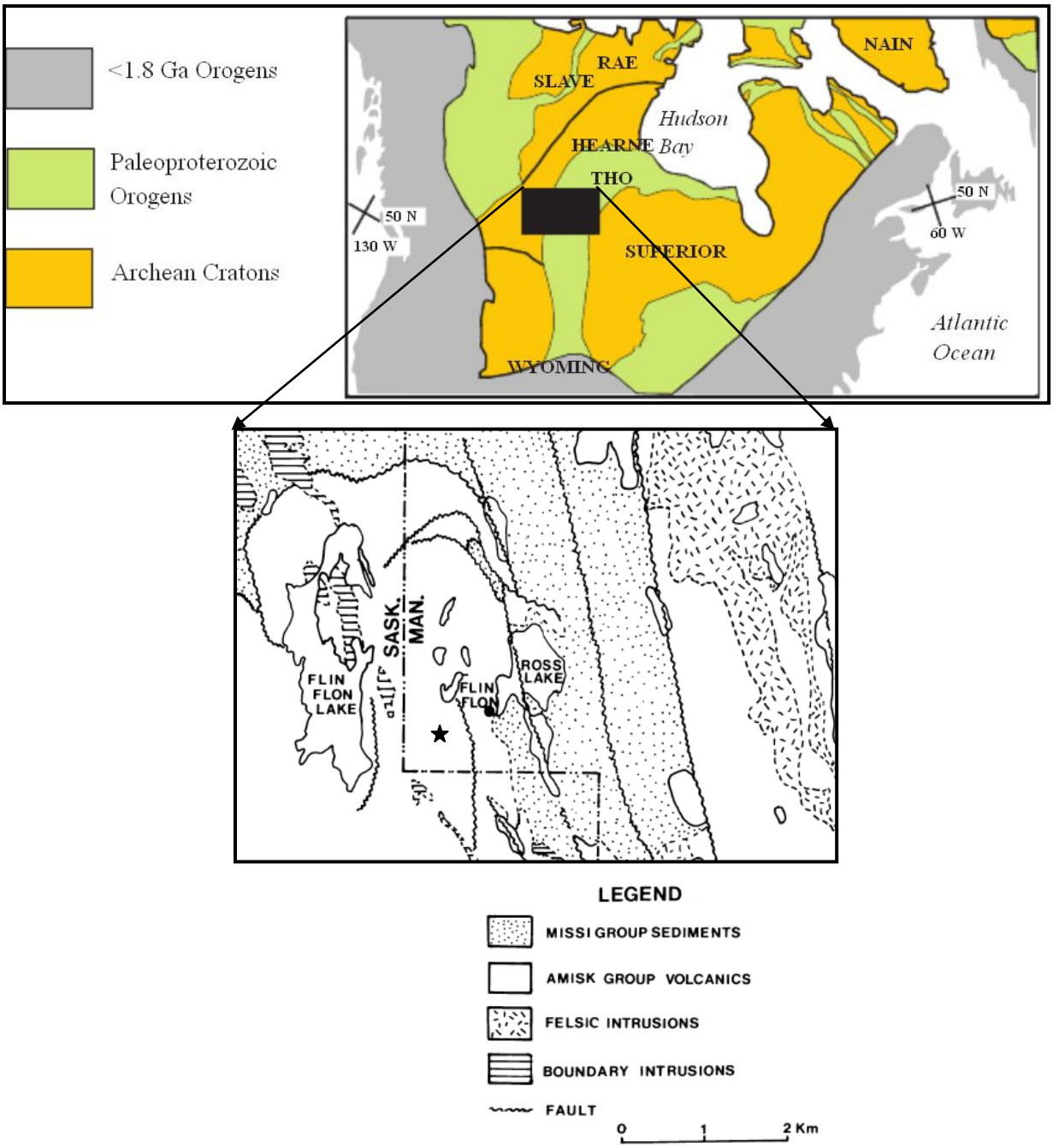

Figure 3.1 Location of drill core and galena (Thorpe, 2008)- fill circle and filled star, respectively. Figure adapted from Galley et al 2007 (Top), and Holland et al (1989) (bottom).

4 ANALYTICAL METHODS

Whole-Rock Lead-Lead Isotope Analysis

Twenty-nine powdered samples from a 32-meter drill-core extracted from the Flin Flon area were analyzed to determine Pb isotopic compositions, and U, Pb concentrations. Concentrations were determined using the Isotope Dilution technique, with enriched isotopes of ^{205}Pb-^{235}U GSU-spike (spike composition of ^{205}Pb=0.77%, and ^{235}U=0.98%). Sample powders were digested in HF and HNO_3 acids for releasing of Pb and U; chemical separations of lead was possible by anion-exchange column chemistry, following the procedures outlined by Krogstad and Walker (1996) (see Appendix 1 for procedures). Analyses were made in the Isotope Geochemistry laboratory at Georgia State University on a ThermoFisher Scientific MAT Element 2 high resolution inductively coupled plasma mass spectrometer (HR-ICP-MS). Total analytical blank averaged 455 picograms (10^{-12}) in weight during the analysis of samples. Therefore, blank correction to the samples was not necessary because of the small amount contained in the analytical blanks. Six replicate analyses of reference standard lead, SRM-982 and SRM-981 from the National Institute of Standards and Technology (NIST), were determined in order to estimate precision and accuracy for the analyses. ^{208}Pb/^{206}Pb isotopic values of SRM-981 were corrected to ^{208}Pb/^{206}Pb known isotopic value (1.00016) of SRM-982 (equal atom lead). Corrected values of the lead standard SRM-981 were compared to their recommended isotopic values (Appendix 3). Thus, precision (2σ) yielded 0.32%, 0.21%, and 0.32%; and accuracy yielded 99.9%, 99.9%, and 99.9% for ^{206}Pb/^{204}Pb, ^{207}Pb/^{206}Pb, and ^{208}Pb/^{206}Pb respectively. Repeated analyses of lead standards suggested that mass fractionation could be corrected using either a power or linear law (Rehkamper and Mezger, 2000).

In this study, in order to quantify the extent of loss of U under oxidizing paleo-weathering conditions, first, measured whole-rock chemical Th/U (κ) and U/Pb (μ)ratios were compared to Time-integrated Th/U ($\kappa^{\dagger}$) and U/Pb ($\mu^{\dagger}$) required for producing the observed Pb isotope signature. Second, CIA (Chemical Index of Alteration) and PIA (Plagioclase Index of Alteration) was used to determine the least weathered rocks or parent rocks. Third, if (κ) and (κ†) or (μ)and (μ†) were different, then U was mobilized from the parent rock. Therefore, the parent rock is corrected for the amount of U lost or gained due to post-alteration; otherwise, no correction is necessary to the amount of U in the parent rock. Third, an element of constant concentration is identified in the profile and used as a normalizing element for the determination of percentage gain or loss of U and some major elements through the profile Gresens (1967).

The decay constants (λ) used were 1.55125 $x10^{-10}y^{-1}$and 4.9475 $x10^{-11}y^{-1}$for ^{238}U and ^{232}Th, respectively. For the derivation of κ and μ, initial Pb isotopic ratios of 15.34, 15.14, and 34.91 respectively for $^{206}Pb/^{204}Pb$, $^{207}Pb/^{204}Pb$, and $^{208}Pb/^{204}Pb$were used from Thorpe (2008). Initial isotopic values were found by analyzing galenas from the Flin Flon mine (Latitude: 54.76722; Longitude:-101.88222).Th/U (κ), and U/Pb (μ) ratios were calculated using radiogenic isotopes ^{238}U and ^{232}Th because of their higher abundance in nature 99.3% and 100%, respectively. Also, isotopic ^{204}Pb was used because it is a stable isotope and has a constant natural abundance.

As suggested by Pollack et al. (2009), in a $^{206}Pb/^{204}Pb$ - $^{208}Pb/^{204}Pb$ diagram, κ values would represent slopes, where κ=0 (horizontal variation) and κ=∞ (vertical variation) represent addition of U or depletion of Th to the system, respectively. In the case of Missi sediments overlaying the paleosol, reference Pb isotope growth-model values from Kramers and Tolstikhin (1997) are compared to observed values to account for gains or losses of U, considering that the

Th concentration remains unchanged. Paleosols are compared to the least altered average values from parent basal volcanics.

The age of the suite of rocks is obtained by measuring the slope in a $^{206}Pb/^{204}Pb$ - $^{207}Pb/^{204}Pb$ diagram. These long recognized lead isotopic ratios are used in age determinations because the two radioactive parent U isotopes decay at different rates, causing a unique time-dependent relation between them (Faure and Mensing, 2005). If the $^{206}Pb/^{204}Pb$ - $^{207}Pb/^{204}Pb$ diagram shows the scattering of points along a linear slope, then extraneous radiogenic lead was added to the system; thus, lead isotopic ratios are not able to define an age to the system. Ages were calculated using IsoPlot 3.0 (Ludwig, 2001)

The Isochron diagram $^{238}U/^{204}Pb$ vs. $^{206}Pb/^{204}Pb$ is used to obtain the slope and can also define an age for the suite of rocks studied, with the condition that they remained closed to fractional changes of U. If the samples plot in a linear array, they are considered to have a closed system behavior. Any deviation or scattering from the slope would indicate either a gain or loss of U from the rock, assuming the redox sensitive behavior of U (Rosholt et al., 1973).

Major Element Analysis

Major element analysis was performed on 29 powdered samples from a 32-meter drill-core extracted from the Flin Flon area with the purpose of measuring chemical compositions of sediments, paleosols, and parent volcanic rock contained along the drilled core. Chemical compositions were used to determine alteration indexes and chemical variations along the profile. Chemical compositions were obtained by measuring major element oxide concentrations by X-Ray Fluorescence (XRF) using an automated Rigaku 3270 X-ray Spectrometer fitted with a Rhodium X-ray tube operated at 50 kV and 50 mA, at the Georgia State University's

Geosciences Department. See Appendix 2 for a sample-fused glass preparation and Loss on Ignition (LOI) procedures.

Multiple measurements of the deepest sample in the drill-core are used in the determination of precision in order to assess the variation of the instrument in repeated measurements. Precision (2σ, n=10) yielded an average of 0.80%, >0.01%, 1.21%, 1.02%, 0.00%, 1.91%, 0.75%, 4.06%, 6.38%, >0.01% for SiO_2, TiO_2, Al_2O_3, Fe_2O_3, MnO, MgO, CaO, Na_2O, K_2O, P_2O_5, respectively. Accuracy was determined by replicate measuring of basalt reference disk BHVO-1 from the United States Geological Survey (USGS). Average accuracy (n=11) yielded 99.98%, 99.97%, 99.98%, 99.98%, 99.94%, 99.91%, 99.97%, 99.31%, 99.79%, 99.45% for SiO_2, TiO_2, Al_2O_3, Fe_2O_3, MnO, MgO, CaO, Na_2O, K_2O, P_2O_5, respectively. See Appendix 4 for measured values.

Molecular proportions are used in the plotting of A-CN-K and (A-K)-CaO*-NaO diagrams. Molecular proportions of cations are calculated by dividing each oxide constituent by the formula weight of the oxide (i.e., Al_2O_3= (Al_2O_3 wt%) /101.96). Al_2O_3, CaO, Na_2O, K_2O molar proportions were normalized to 100% for the plotting of A-CN-K and (A-K)-CaO*-NaO diagrams.

5 RESULTS

Whole-Rock Lead-Lead Isotope Analysis

Precise measurement of accumulated radiogenic Pb isotope ratios in whole-rock samples were used to calculate present chemical U/Pb (μ) ratio in the parent volcanics and paleosol. Also, by employing Lead-Lead systematics, Time-integrated Th/U ($\kappa^{\dagger}$) and U/Pb ($\mu^{\dagger}$) ratios (ratios at the time of formation or deposition) were calculated using the calculated age for the system.

Table 5.1 presents whole-rock Pb isotopic composition, U/Pb (μ) measured chemical ratios, calculated and required U/Pb ($\mu^{\dagger}$) and Th/U ($\kappa^{\dagger}$) values for lead isotopic composition for an age of 1906 Ma. Th/U (κ) reference ratio for average upper crust value from Taylor and McLennan (1985), and U variation [(μ measured/ μ calculated or reference) -1]. U changes in (ppm) were calculated using the formula (measured U (ppm) * ΔU%)/(100-(absolute ΔU%)).

Relative U variation for the parent of sediments at the time of deposition was calculated as the difference between the average Th/U (κ=3.86) upper crust ratio predicted by the Kramers and Tolstikhin (1997) Pb isotope growth model and the Time-integrated Th/U ($\kappa^{\dagger}$) ratios calculated from whole-rock radiogenic Pb ratios. There is dissimilarity between the Th/U upper crust ratio and the Time-integrated Th/U ratio of samples; thus, there was a potential U addition to the sediments at the time of deposition. Time-integrated Th/U ratios relative to the upper crust ratio range from 46.8% to 70.4%, 58.9% average (1.89 ppm average). For the estimation of U variation in the volcanics (parent rock of paleosol) at time of emplacement, observed U/Pb (μ) was compared to calculated time-integrated U/Pb ($\mu^{\dagger}$) using an age of 1906 Ma, which is the calculated age of the parent volcanics (Figure 5.1). Least weathered samples of the volcanics show no variation when comparing time-integrated and observed U/Pb ratios (0 ppm average), therefore no U correction was necessary for the volcanics (paleosol's parent rock). Highest

dissimilarity between the Time-integrated and observed U/Pb ratio was found in the corestone sample, -0.16ppm. Due to the onion skin texture of corestone (sample #18), this sample ought to be the least weathered sample in the paleosol zone (see Table 5.1).

Figure 5.2 shows Time-integrated Th/U ($\kappa^{\dagger}$) vs. depth. Volcanics have an average $\kappa^{\dagger}$ of 2.0, plotting close to the average reference line of κ=2.21 for the Aleutians arc (Sun, 1980). Lower paleosol samples plot to the right of average $\kappa^{\dagger}$=2 for volcanics and the Aleutians arc reference line, indicating a decrease in U concentration at the time of formation, considering that Th behaves conservatively under oxidative weathering (Krogstad, 2004). In contrast, upper paleosols plot to the left of average $\kappa^{\dagger}$=2 for volcanics and the Aleutians arc reference line, indicating addition of U to those samples at the time of formation or shortly after. Sediment samples have an average $\kappa^{\dagger}$ of 1.59, plotting to the left of the average upper crust reference line (κ=3.8). Typically sediments plot near the average upper crust reference line, but in this case U addition appears to have lowered κ values at time of deposition or shortly after.

Figure 5.3 shows time-integrated $\kappa^{\dagger}$ vs. observed 1/μ, (Th/U vs. Pb/U). In this diagram, a qualitative description of the behavior of U is possible since measured Pb/U ratios are used. U loss should plot away from the origin following a diagonal line; while U gain will plot towards the origin. Pb gain will follow a vertical line away from the origin. Volcanics plot close to the Aleutian's arc reference value and show some dispersion from the average volcanic values; volcanics have a $\kappa^{\dagger}$ of 2.0 average and $1/\mu^{\dagger}$ of 0.08 average Lower paleosols plot the furthest away from the origin, indicating that U loss was greater in those samples than in the upper paleosol relative to average ratios for volcanics. In contrast, sediments appear to have gained U at the time of formation relative to average upper crust values and volcanics. Also, Pb concentration is higher in the lower paleosol than lower paleosol and volcanics; corestone

sample is the most enriched in Pb (10 ppm). Pb is also enriched in the upper paleosol (3.68 ppm average) relative to the average volcanics, but not as much as the lower paleosols. In contrast, sediments appear to have a minor Pb loss compared to upper crust and volcanics.

Conventionally, $^{206}Pb/^{204}Pb$ vs. $^{207}Pb/^{204}Pb$ diagrams for whole-rock isotopic composition has been used to determine the radiometric age of a system, as long as the system has remained chemically closed to U and Pb throughout its history. A radiometric age of 1906±540 Ma (MSWD=7.1) was calculated for the volcanic (Figure 5.1$^{206}Pb/^{204}Pb$ vs. $^{207}Pb/^{204}Pb$ diagram). Also, radiometric ages for paleosols and sediments were calculated; paleosols and sediments display an age of 2173±470 Ma (MSWD=3.4) and 1920±120 Ma (MSWD=2.5), respectively (Figure 5.5, 5.6).

The evaluation of uranogenic or thorogenic Pb growth (Pollack et al., 2009) is possible by using $^{206}Pb/^{204}Pb$ and $^{208}Pb/^{204}Pb$ ratios, shown in Figure 5.7. Horizontal variations would indicate uranogenic Pb growth, while vertical variations would indicate thororogenic Pb growth. Volcanics have a $\kappa^{\dagger}$=2 average (see Table 5.1); therefore, in Figure5.7, a ray of $\kappa^{\dagger}$=2 is constructed starting from the initial Pb isotopic ratio obtained from galenas representative of the area of study. As indicated by Krogstad (2004), in the absence of oxidative weathering the arrangement of data would plot along the constructed ray. It is observed that paleosols present scattering along the constructed ray, indicating decoupling of U from Th in the paleosols. Lower paleosols plot farthest to the left, and upper palesosols plot closer to the ray $\kappa^{\dagger}$=2 (volcanics) from the average volcanic slope; therefore, indicating that lower paleosols lost more U than the upper paleosols. Paleosols, in the same diagram, plot below the array of volcanics, indicative of small amounts of radiogenic Pb in these samples. Sediment samples present variability in $\kappa^{\dagger}$

values relative to the Pb isotopic growth model proposed by Kramers and Tolstikhin (1997), κ=3.86, indicating U gain in the sediments relative to the reference growth model.

Observed Pb/U (1/μ) on paleosol samples is compared to degree of weathering (CIA) in order to assess the trend of U mobility as a function of weathering intensity. Figure 5.4 shows a dashed line depicting an expected U loss trend for oxygenated weathering. This diagram shows an opposite trend than the expected behavior of U as a function of weathering. There is an upwards increase of U (solid arrow) from lower to upper paleosol.

The U-Pb whole-rock isochron ($^{238}U/^{204}Pb$ vs. $^{206}Pb/^{204}Pb$) is based on the accumulation of Pb radiogenic isotopes by decay of the respective parent ($^{238}U \rightarrow {}^{206}Pb$). Given that the rock remained closed to U and Pb, the slope of the isochrones defines the age of the system. In Figure 5.8, an isochron of age 1906 Ma for the volcanic is drawn starting at the initial Pb isotopic ratio. In this Figure, paleosol data points are displaced from the reference isochron, indicating losses of U. The lower paleosols (points 18, 19, 20, 21) present the highest loss of U in the profile; while upper paleosol (with a higher degree of weathering than lower paleosols) show an array that plots closer to the reference isochron, showing gain of U relative to volcanics' isochron. A reference line (dashed line in Figure) is drawn to indicate the minimum loss of U that the paleosol may have experienced.

Major Element Analysis

Table 5.2 shows abundance (in weight percent) of major chemical elements present on sample-fused glasses. Oxide totals for most of the sample-fused glasses do not add up to 100%; such measurement irregularity could be attributed to XRF instrument calibration. By examining Appendix 4, average oxide values for 11 analyses of the BHVO-1 reference glass disk do not agree with accepted values for the reference disk. Nearly all the error is due to low

measurements of SiO_2, leading to low totals for a number of samples. The main goal in major element analyses for this study is to obtain major chemical abundances of K_2O, Na_2O, CaO, and Al_2O_3 for the calculation of index of alteration and TiO_2 for percentage relative changes of the parent rock. The element oxides in consideration closely agree with reference standard values, so are valid for CIA and PIA calculations. Due to the identified error in SiO_2measurements, SiO_2oxidevalues will not be considered for this study.

After converting, K_2O, Na_2O, Fe_2O_3, and MgO into molar proportions and normalizing them to 100, they were plotted in an AFM diagram (Alkalis (K_2O+Na_2O), Fe_2O_3, MgO). Volcanic samples plotted on the Tholeiitic Basalt field (Figure 5.9); such finding is consistent with the description of Holland et al., (1989) corresponding to the oldest Amisk volcanic rocks.

In the assessing of relative changes of a rock, Gresens (1967) formula requires the assumption of a specific immobile element, such as Al, Ti, and Fe. These are commonly conserved in the soil profile during weathering due to their high ionic potential, but Al and Fe are known to move during pedogenesis (Dickie, 2010).Examination of instrument precision for these three elements in the Flin Flon profile shows that TiO_2, Al_2O_3, and Fe_2O_3 have an analytical precision of>0.01%, 1.2%, and 1.0%, respectively (see Appendix 3), thus Ti shows the highest precision in measurement. Also, Figure 5.10 shows that TiO_2 behaves constant through the profile. Therefore, in order to assess the gain or losses of elements through the profile, $TiO_2$is assumed to be constant and is used as a normalizing element in the formula proposed by Gresens (1967) (also, Nesbitt, 1979; and Grant, 1986). In this formula, major oxides and U are normalized to Ti in order to assess percentage elemental changes ratios (gain or loss) of altered samples relative to the unaltered sample (see Table 5.3 for values). In the calculus of percentage elemental changes for Missi sediments, calculated oxides were compared to average values for

upper crust (Taylor and McLennan, 1985); upper crust is considered as the unaltered (parent) sample. This choice responds to the fact that sediments have different provenance; in this study, provenance sources are not characterized. Therefore, a comparison between sediment oxide values and average upper crust values provide insight into the relative elemental changes. Although average upper crust values are not the "true" parent for sediments, but is considered as a uniform proxy against which the profile can be compared. As for the paleosol, average composition values of the least altered volcanics (last 2 samples from the drill-core) were used as the unaltered sample to normalize values of paleosol samples in order to determine percentage elemental changes. Paleosol samples were divided in upper (six upper samples) and lower paleosol (four lower samples) in order to better evaluate alteration changes.

Chemical variations in Ca and Mg relative to Al are evident in the profile and relate well to the stratigraphic column of the drill core for the Flin Flon area (Figure 5.10). Also, it shows the more conservative behavior of TiO_2 in the profile compared to Al_2O_3.Figure 5.11 shows a comparison of Chemical Index of Alteration (CIA) and Plagioclase Index of Alteration (PIA) for sediments, the paleosol, and volcanics within the profile. From this diagram, PIA and CIA show similar values for volcanics as well as lower paleosols; but upper paleosols and sediments show dissimilar trends.

Ca/Ti (Figure 5.12A) shows upward depletion of Ca from the lower to upper paleosol as weathering increased: CIA from 46% to 75%. Ca loss ranges from -92% to -41% (-71% average) for the upper paleosol, and from -76% to 28% (-30% average) for the lower paleosol relative to the least weathered Amisk volcanics. Sediments also show depletion of Ca with weathering increase: CIA from 65% to 76%; losses range from -40% to -96% (-78%average) relative to average upper crustal values (Taylor and McLennan, 1985).

Na/Ti (Figure5.12B) shows upward depletion of Na from the lower to upper paleosol. At the upper paleosol, for CIA values ranging from 61% to 75%, Na loss ranges from -95% to -100% (-99% average)relative to the least weathered Amisk volcanics. The lower paleosol shows an upward gradual depletion of Na for CIA values from 46% to 67%; Na loss rangesfrom 34% to -13% (11% average) relative to the least weathered Amisk volcanics. Sediments show total depletion of Na (100% average)for CIA values ranging from 65% to 76%, relative to the average upper crustal values (Taylor and McLennan, 1985).

K/Ti (Figure 5.12C) shows the upward increment of K from the lower paleosol to the upper paleosol. In the upper paleosol, as weathering increases (CIA from 61% to 75%), K increment ranges from 651% to 1405% (987% average) In contrast, the lower paleosol shows K depletion from 13% at the top to -64% at the bottom and -15% in average Both the upper and lower paleosol values are relative to the least weathered volcanics. Sediments showupward depletion of K;K values range from 62% at the bottom to -87% at the top (-28% average),relative to average upper crustal values (Taylor and McLennan, 1985), for CIA values ranging from 65% to 76%,

The parent rocks for paleosol and sediments were corrected to calculate U present in the parent rock at the time of deposition/emplacement. The U concentration of the parent rock for sediments (upper crust values) was increased by 1.89 ppm (average U gain in sediments at or shortly after deposition), while no correction was needed for the parent rock of volcanics (the least two altered samples had U mobility of 0 ppm average.).U/Ti (Figure 5.12D) shows upward increments from lower to upper paleosol. In the lower paleosol (CIA 46%-67%), U losses range from -1% to -38% at the top (-17% average). In the upper paleosol, there is an upward increment of U (11% average) as the degree of weathering increases; -48% to 60%. Therefore, U

concentration is increased at the top of the upper paleosol zone, and at the upper part of the lower paleosol zone, relative to the least weathered volcanics (parent). Sediments show depletion of U as weathering increases (CIA from 65% to 76%). U losses range from -71% to -94% (-84average), relative to average upper crustal values (Taylor and McLennan, 1985).

Weathering trends were evaluated using ternary compositional diagrams. A-CN-K (Figure 5.13) and A-C-N (Figure 5.14) diagrams were plotted using normalized molar proportions. In the A-CN-K (Figure5.13) diagram, the point plotting the farthest away from the Al apex is considered as the least weathered sample, while the point plotting nearest is considered to be the most weathered sample. Also, in this diagram, a red solid arrow denotes the expected weathering trend of volcanics increasing towards the Al apex (Al being less soluble than alkalis). To the right of the expected weathering trend, K is added to the samples, and to the left, K is depleted. Volcanic samples plot next to the A-CN boundary, and the deepest sample in the drill-core plot furthest from the Al apex. Close to the deepest volcanic sample plots the cornerstone sample, which is the least weathered sample in the paleosol. Volcanic samples show first, quick minor depletion of K relative to the average volcanic composition (volcanics plot on the A-CN boundary), followed by depletion of Ca and Na as CIA values increase (indicating a higher degree of weathering). The lower paleosol (4 samples) plot along the A-CN boundary, and then gradually show increases in K up to the weathering trend arrow with increasing CIA values. At higher weathering values, the upper paleosol samples plot to the right of the weathering trend arrow, thus showing the addition of K to these samples. The addition of K to the upper paleosol samples shows “unreal”(post-alteration effects on maximum reached) CIA values (60-75%). By extending a line from the K apex towards the weathering trend arrow (Fedo et. al., 1995), it is possible to define maximum CIA values (68-94%) corresponding to the pre-

addition of K to such samples. Sediments are compared to upper crust values (Taylor and McLennan, 1985); a solid blue arrow passes through the upper crust reference value, indicating its expected weathering trend. Only one sediment sample plots on top of this weathering trend, while the rest plot to the right of this arrow. As in the upper paleosol samples, sediments show addition of K, thus observed CIA values in sediments are "unreal". Pre-addition of K gives maximum CIA values ranging from 72 to 85%.

The PIA compositional diagram (A-C-N) (Figure5.14) presents plagioclase elemental changes as a function of the degree of weathering (PIA values). The deepest drill-core sample (volcanic) plots furthest away from the Al-K_2O apex, showing a lesser degree of weathering. With increasing weathering, volcanics show a major depletion of Ca and minor depletion of Na. Likewise, the lower paleosol (four samples) show first depletion of Ca and then some depletion of Na up to PIA ~75%. As for the upper paleosol, with a higher degree of weathering (PIA>75%), Na is completely lost, then the remainder of Ca is lost from the paleosol. All sediments plot on the (Al-K) – CaO* boundary, while the average upper crustal reference value plots near the deepest drill-core sample. Sediments are depleted in Na and Ca, moving towards the Al apex as weathering continues. As in the depletion process of elements from volcanics to paleosols due to weathering, it is speculated that sediments follow the same path.

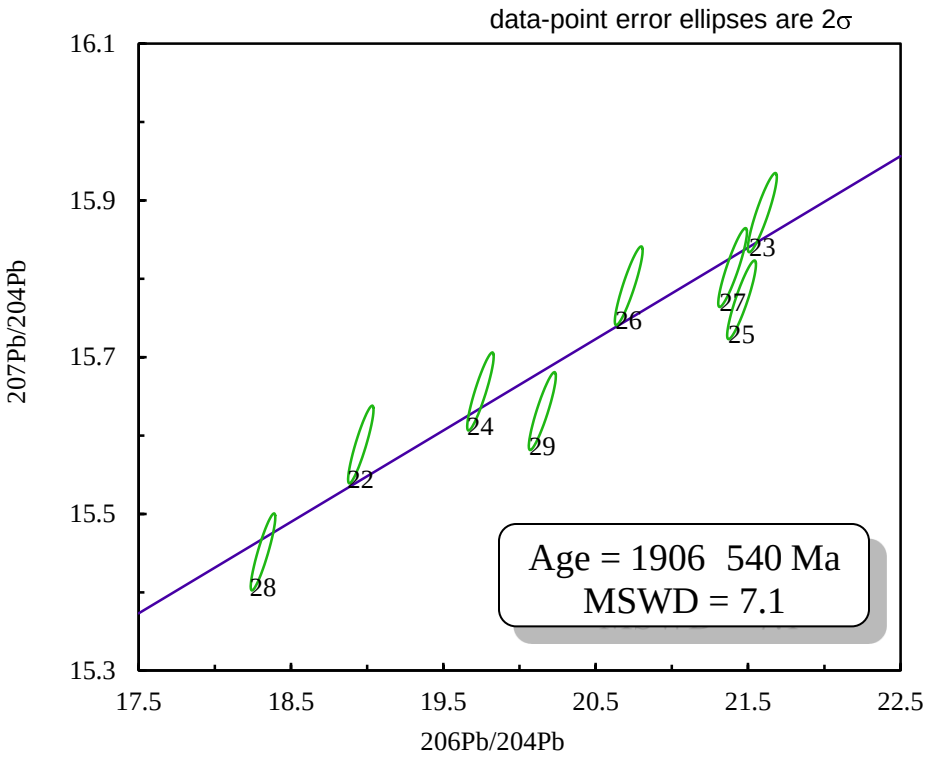

Figure 5.1 $^{206}Pb/^{204}Pb$ vs. $^{207}Pb/^{204}Pb$ whole-rock isotope ratio diagram for volcanic samples. Numbers describe samples (see table 5.1). Almost near array indicates Pb homogenization within the volcanics.

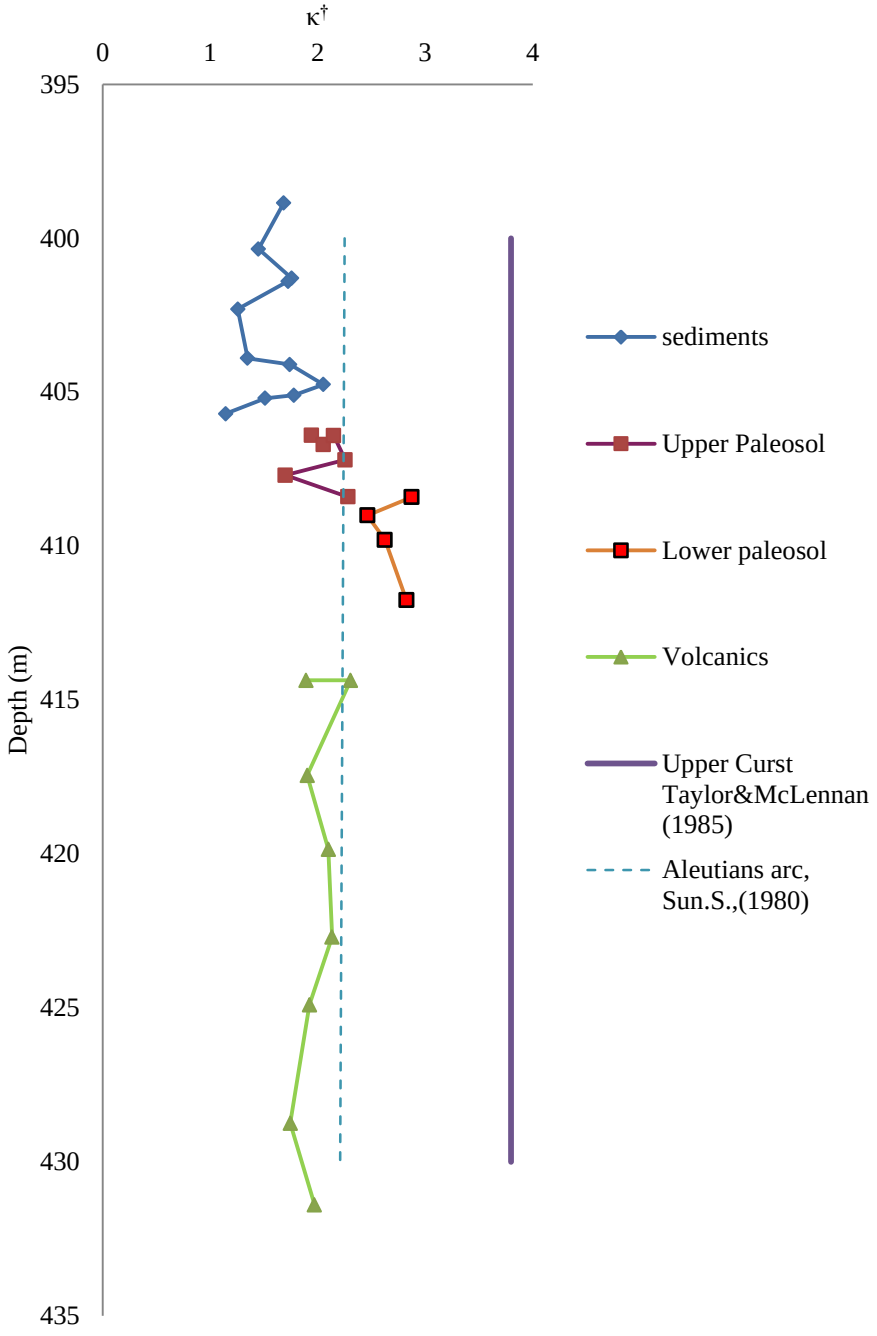

Figure 5.2 $\kappa^{\dagger}$ (Th/U) vs. depth.Upper crust reference value κ =3.8, from Taylor and McLennan (1985). Aleutian's arc reference value κ =2.21, from Sun (1980).Sediments, and paleosols indicate mobility of U at time of deposition.

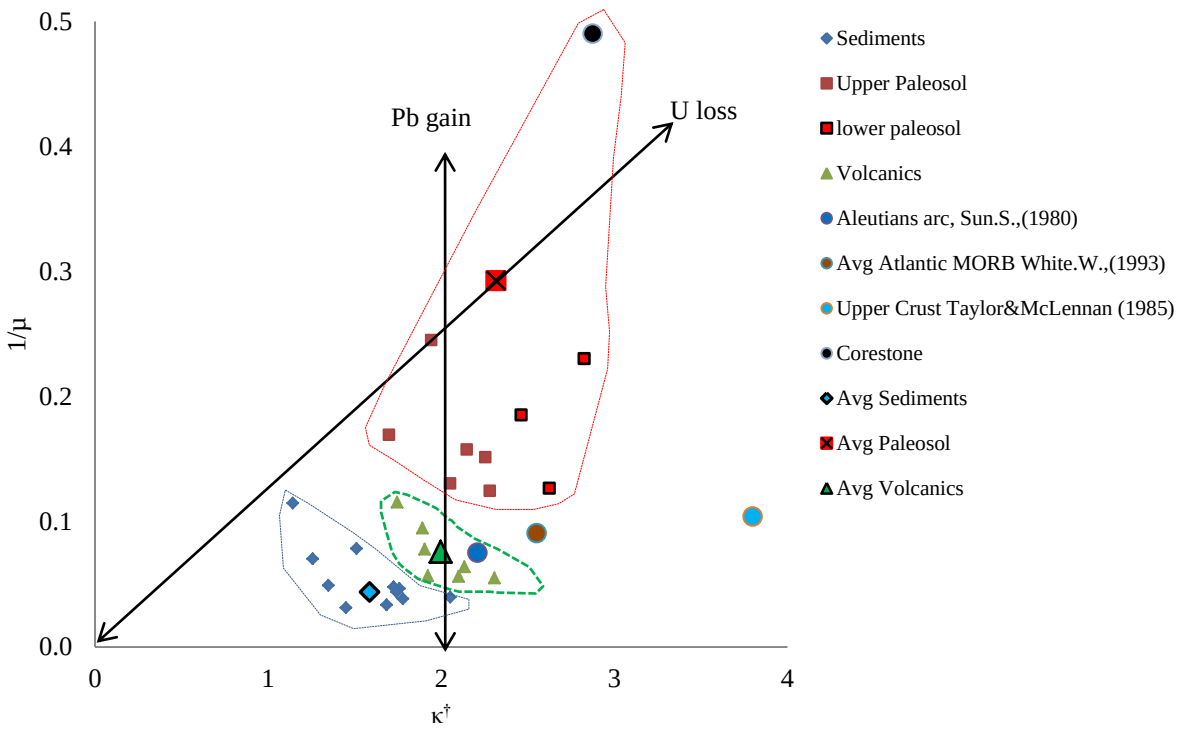

Figure 5.3 Time-integrated Th/U ($\kappa^{\dagger}$) vs. measured Pb/U (1/μ) ratios. Sediments gained U at time of deposition relative to upper crustal values; paleosols lost U relative to volcanics, shortly after formation.

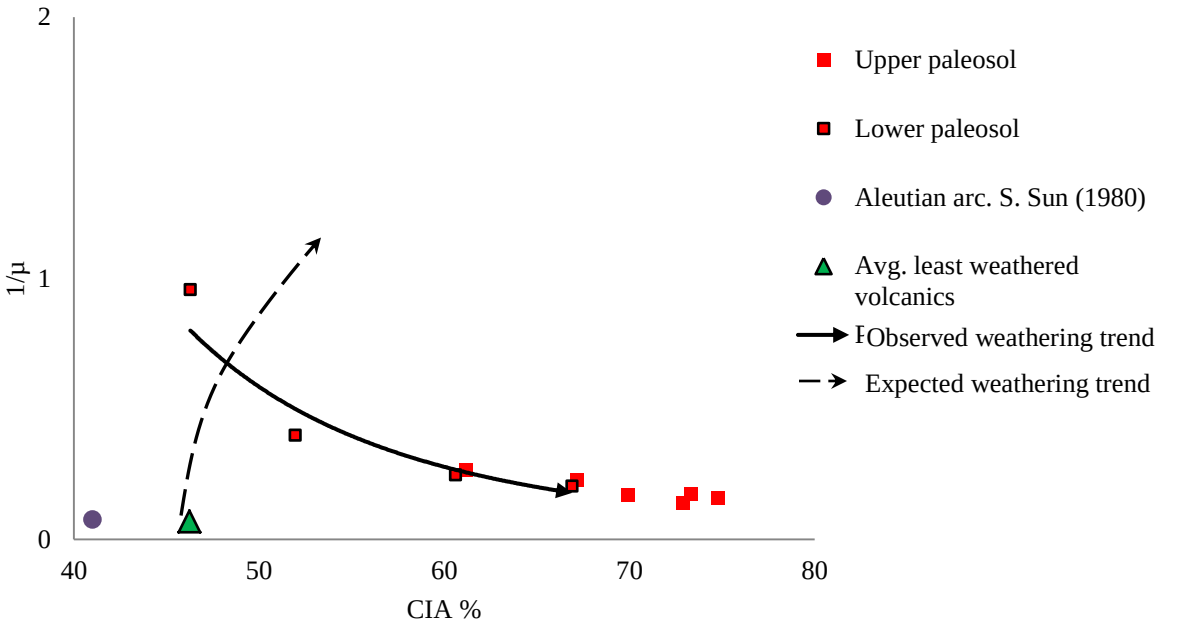

Figure 5.4 Measured 1/μ (Pb/U) vs. CIA, for paleosols. Lower paleosol observed weathering trend follows an exponential regression type, indicating an upward gain of U.

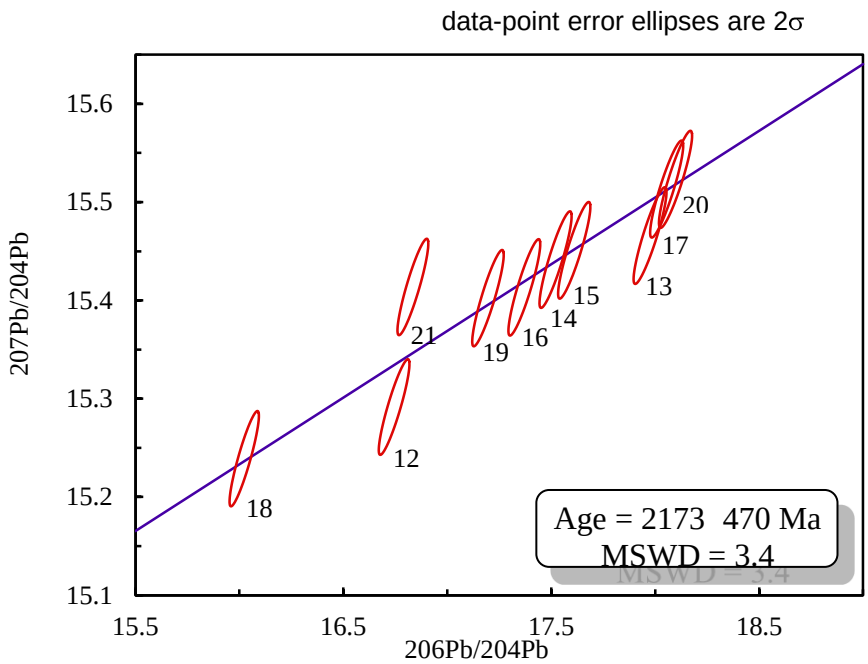

Figure 5.5 $^{206}Pb/^{204}Pb$ vs. $^{207}Pb/^{204}Pb$ whole-rock isotope ratio diagram for paleosol. Almost near array indicates Pb homogenization within the Flin Flon paleosol.

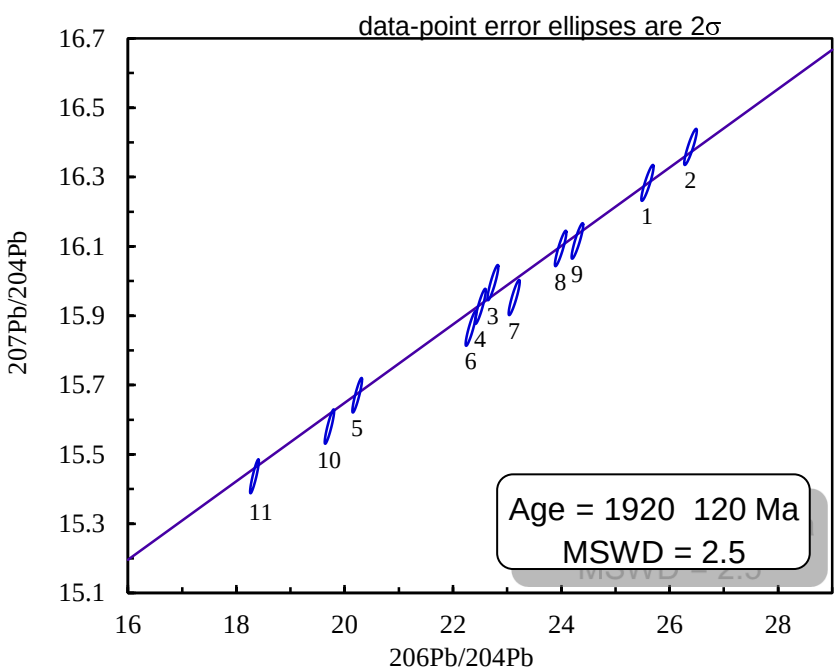

Figure 5.6 $^{206}Pb/^{204}Pb$ vs. $^{207}Pb/^{204}Pb$ whole-rock isotope ratio diagram for sediment. Almost near array indicates Pb homogenization within the Missi sediments.

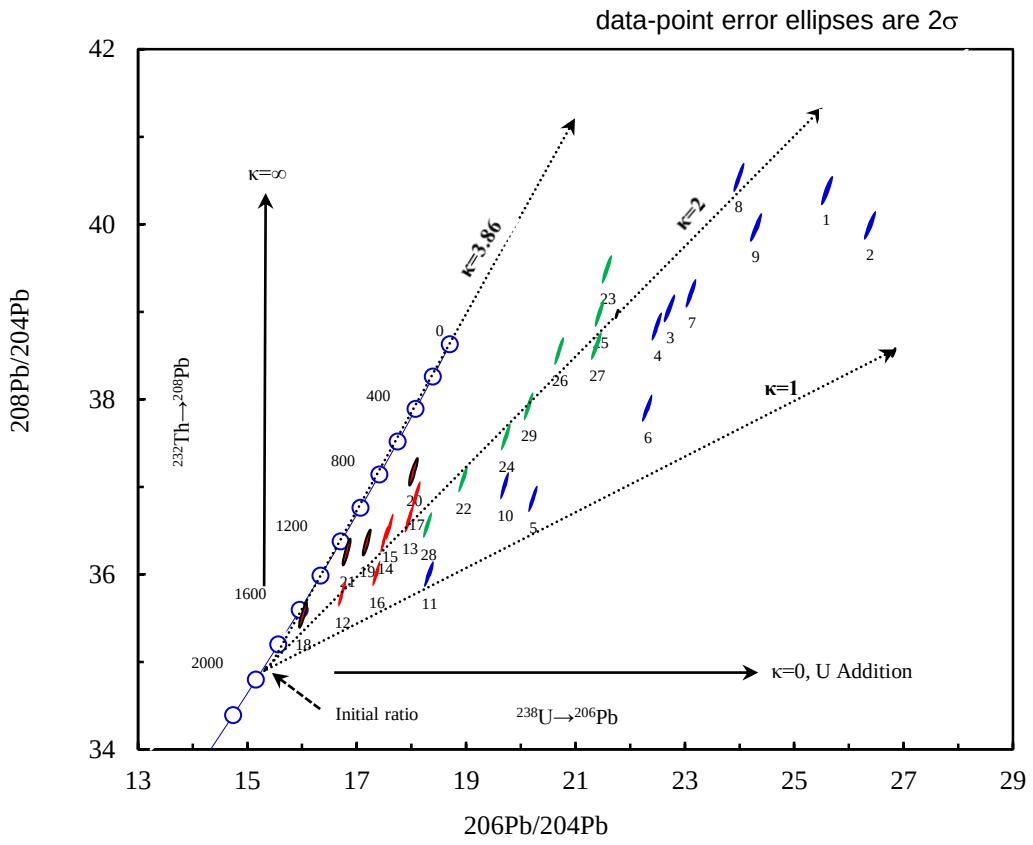

Figure 5.7 $^{206}Pb/^{204}Pb$ vs. $^{208}Pb/^{204}Pb$ whole-rock isotope ratio diagram. Sediments on blue ellipses, upper paleosol on red, lower paleosols are on red with outer black line, and volcanics on green. Growth curve shown represents the Pb isotope growth model of Kramers and Tolstikhin (1997), κ=3.86. Numbers describe samples (see Table 5.1). Initial isotopic ratios are from Thorpe (2008). κ=2 represents the average for volcanics. Uranogenic Pb addition/substraction was higher relative to thorogenic Pb, thus U mobility was high during the Paleoproterozoic.

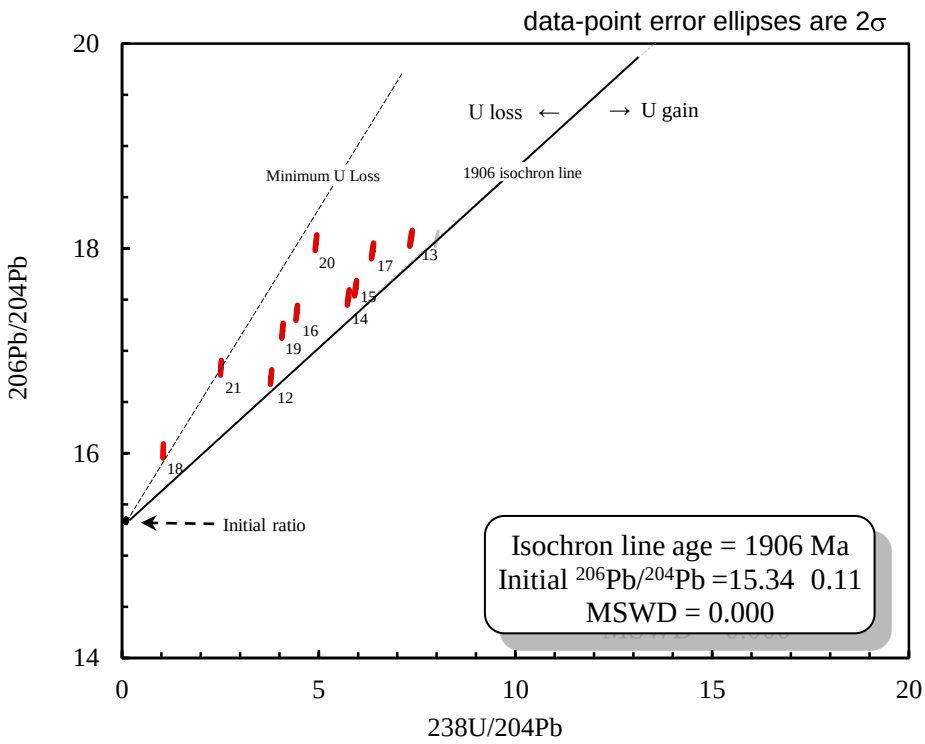

Figure 5.8 $^{238}U/^{204}Pb$ vs. $^{206}Pb/^{204}Pb$ whole-rock Isochron for paleosols and sediments.Isochron line age corresponds to the volcanics average age. Any deviation from the Isochron represents either gain or loss of U. Dashed line indicates minimum U loss that paleosols might have experienced due to weathering.

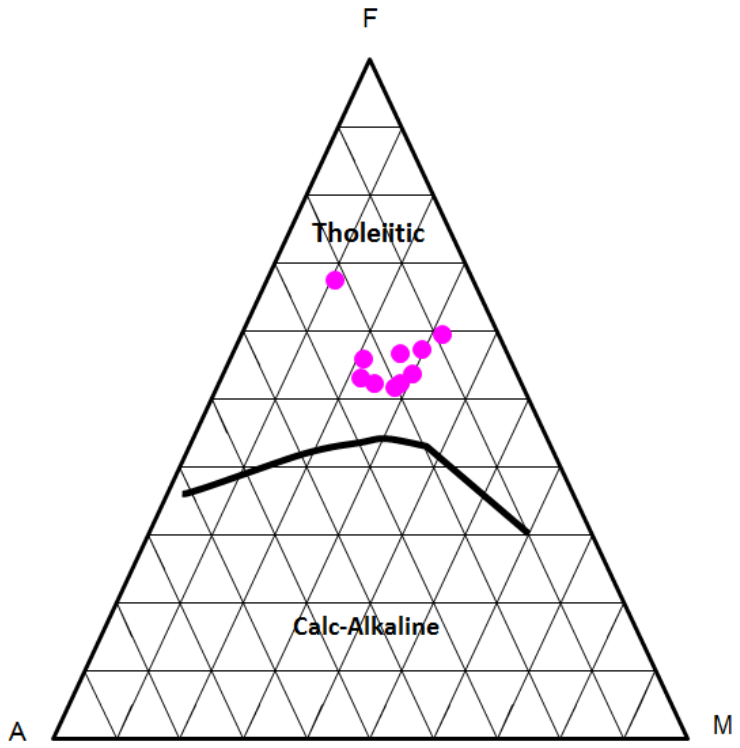

Figure 5.9 AFM diagram, A (Al2O3), F (FeO), and M (MgO), for volcanics of the Flin Flon area. Solid line divides Tholeiitic from Calc-alkaline regions.

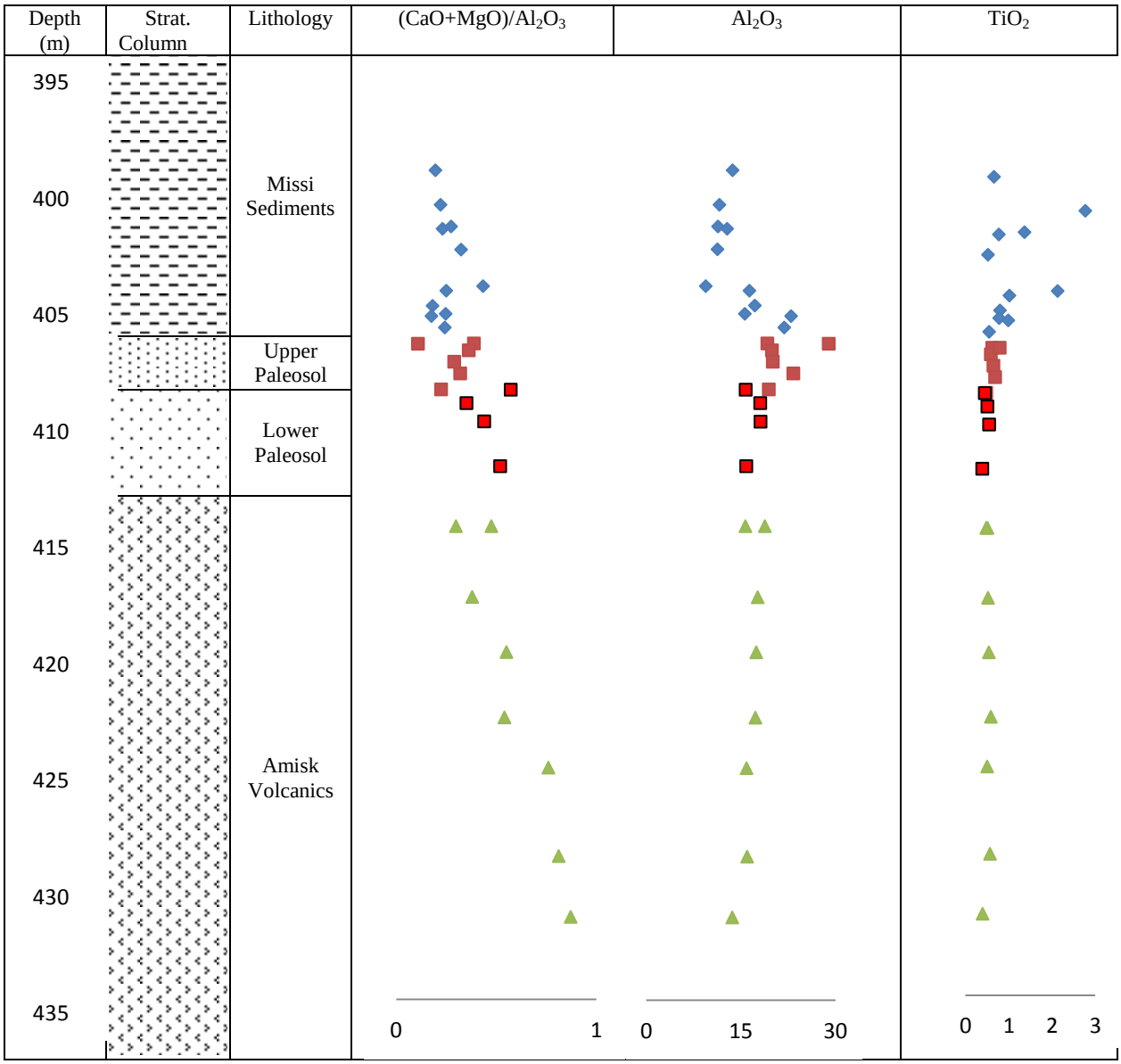

Figure 5.10 Stratigraphic section and profile geochemical variations. Loss of alkaline earths indicates upward weathering increase. TiO_2 behaves more conservative than Al_2O_3within the profile.

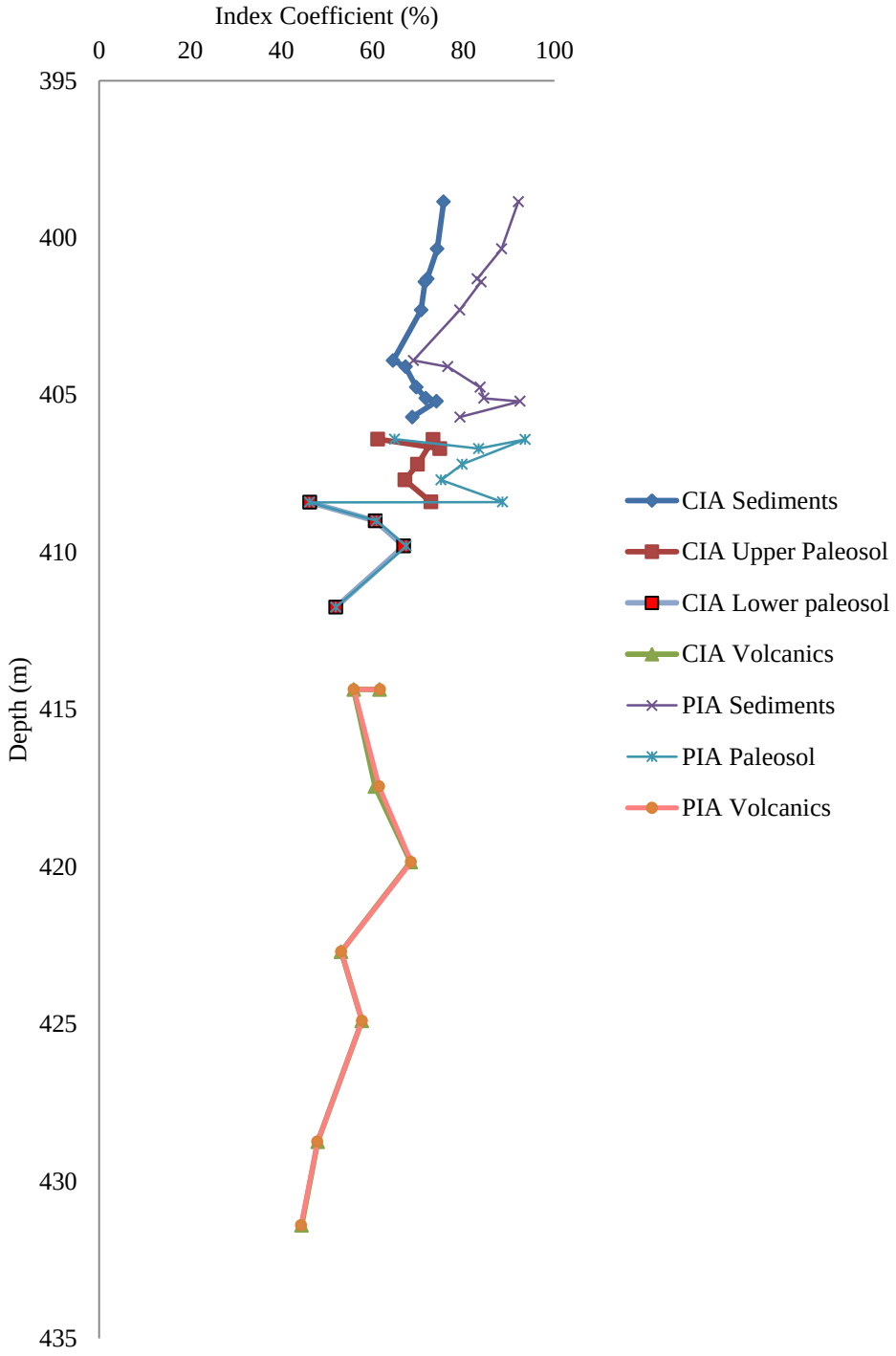

Figure 5.11 CIAand PIA vs. depth. Separation of PIA and CIA trends in upper paleosol and sediments indicate addition of K due to metasomatism.

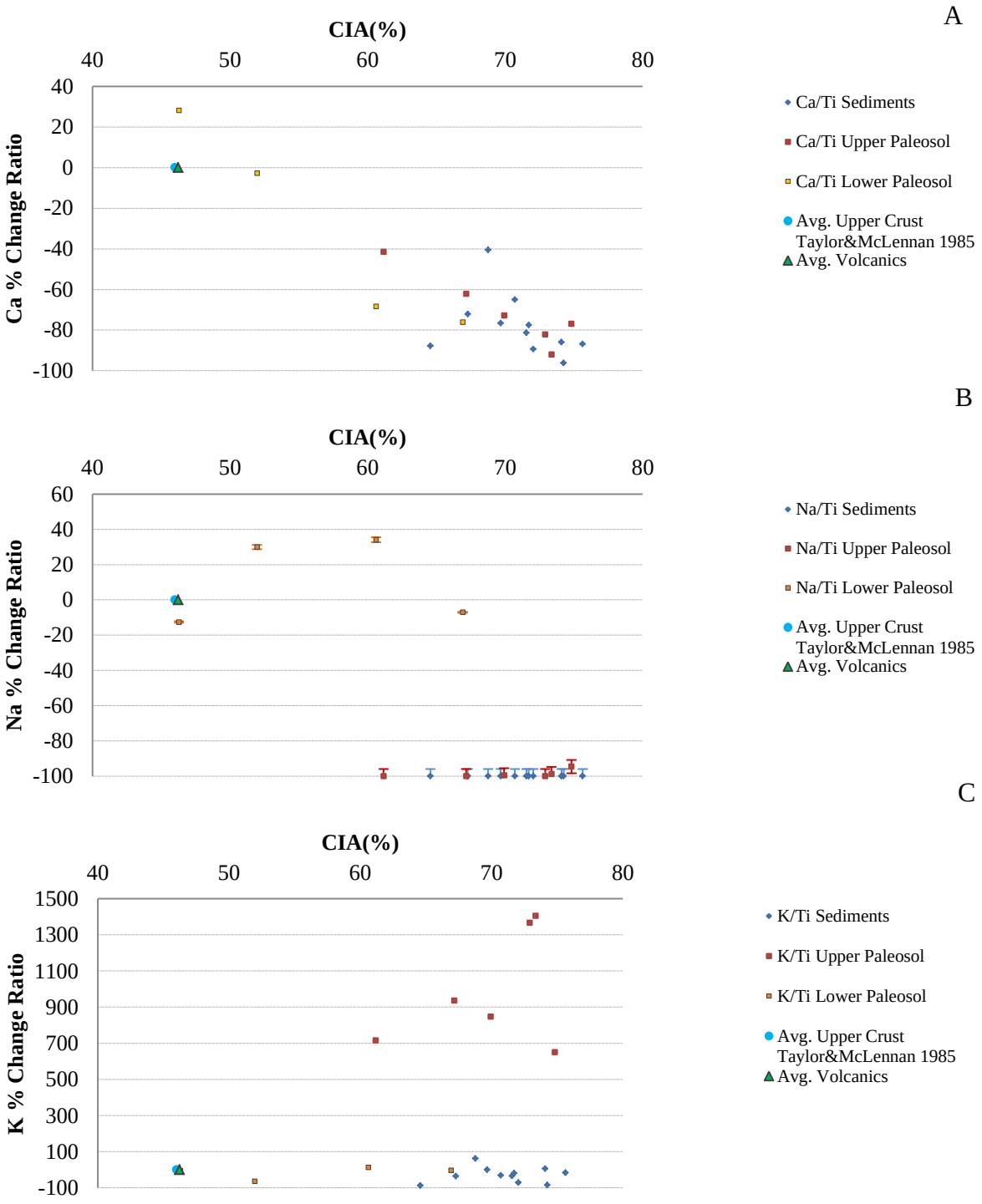

Figure 5.12 (A, B, C) Percentage change (gain/loss) ratios (normalized to TiO2) as a function of weathering intensity (CIA index). Sediments are normalized to average upper crust values (Taylor and McLennan, 1985); paleosols are normalized to the deepest least two weathered samples.Error bars are similar or less than the size of the marker.

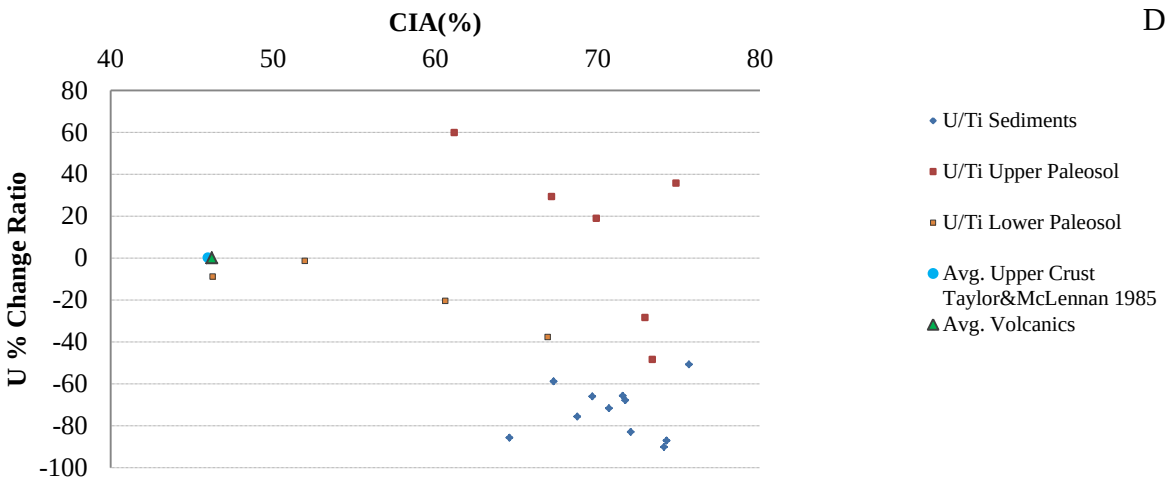

Continued Figure 5.12 (D) Percentage change (gain/loss) ratios (normalized to TiO_2) as a function of weathering intensity (CIA index). Sediments are normalized to average upper crust values (Taylor and McLennan, 1985); paleosols are normalized to the deepest least two weathered samples. Error bars are similar or less than the size of the marker.

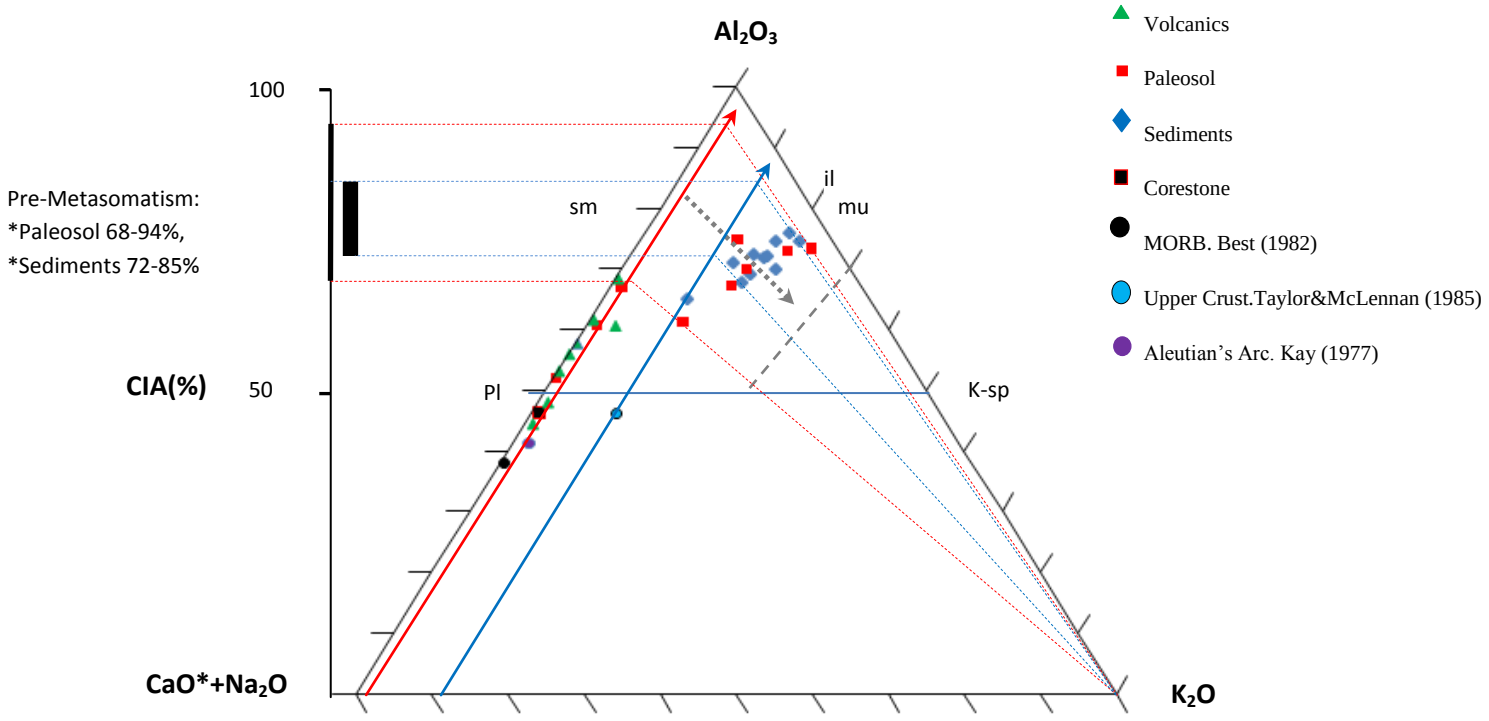

Figure 5.13 A-CN-K diagram (molecular proportion).MORB, Upper Crust, and Aleutians Arc values plotted CaO*(silicate fraction only). Solid red line represents weathering trend; gray dotted line represents K addition trend.

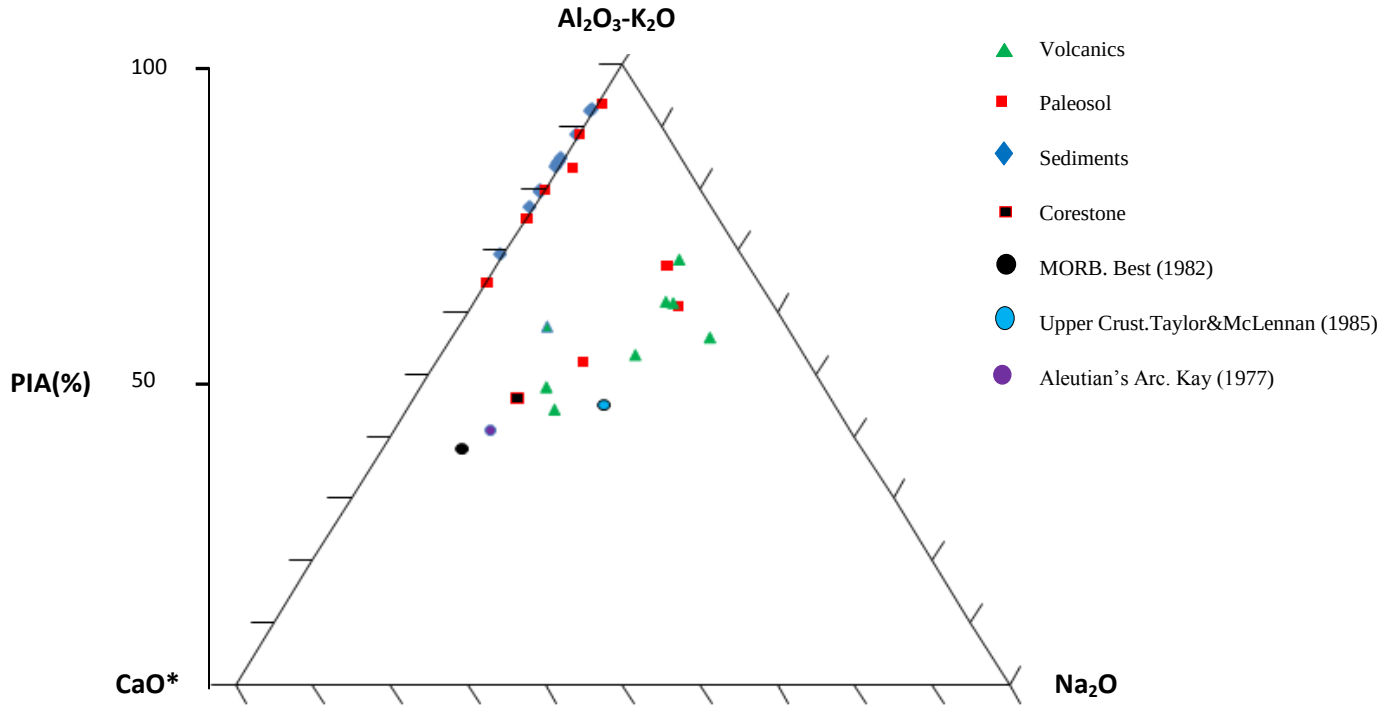

Figure 5.14 (Al_2O_3-K_2O)-CaO*-NaO diagram (molecular proportions). MORB, Upper Crust, and Aleutians Arc values plotted with CaO*(silicate fraction only).

Table 5.1: Measured whole-rock Pb isotopic composition, measured μ (U/Pb), time-integrated $\mu^{\dagger}$ (U/Pb) and $\kappa^{\dagger}$ (Th/U) calculated required values for observed lead composition using age of 1906 Ma, κ (Th/U) average upper crustal ratio of 3.86 predicted by the Kramers and Tolstikhin (1997) for Pb isotope growth model; and ΔU, gain indicated by +, loss indicated by -.ΔU(ppm)=(measured U(ppm) * ΔU%)/(100-(absolute ΔU%)), for measured U(ppm) values see Table 5.2.

	Sample	Depth (m)	$^{206}Pb/^{204}Pb$	$^{207}Pb/^{204}Pb$	$^{208}Pb/^{204}Pb$	$\kappa^{\dagger}$	κ	μ	$\mu^{\dagger}$	ΔU (%)	ΔU (ppm)
Sediments	1	398.85	25.59	16.28	40.37	1.68	3.86	-	-	56.4	2.18
	2	400.35	26.38	16.39	39.98	1.45	3.86	-	-	62.4	3.10
	3	401.30	22.74	16.00	39.03	1.76	3.86	-	-	54.4	1.45
	4	401.40	22.51	15.93	38.82	1.73	3.86	-	-	55.3	1.70
	5	402.30	20.23	15.67	36.85	1.26	3.86	-	-	67.4	1.58
	6	403.90	22.33	15.86	37.89	1.35	3.86	-	-	65.1	2.93
	7	404.10	23.13	15.95	39.20	1.74	3.86	-	-	54.9	2.65
	8	404.75	23.99	16.09	40.53	2.05	3.86	-	-	46.8	1.24
	9	405.10	24.30	16.12	39.95	1.78	3.86	-	-	53.9	1.52
	10	405.20	19.72	15.58	37.00	1.51	3.86	-	-	60.8	0.79
	11	405.70	18.34	15.44	35.99	1.14	3.86	-	-	70.4	1.66
Paleosols	12	406.40	16.74	15.29	35.77	1.94	-	3.79	4.08	-7.2	-0.03
	13	406.70	17.98	15.47	36.62	2.05	-	6.37	7.66	-16.9	-0.07
	14	406.4*	17.52	15.44	36.39	2.15	-	5.75	6.34	-9.3	-0.02
	15	407.20	17.61	15.45	36.53	2.26	-	5.94	6.60	-10.1	-0.04
	16	407.70	17.37	15.41	36.00	1.70	-	4.44	5.91	-24.8	-0.13
	17	408.4 P	18.10	15.52	36.90	2.28	-	7.35	8.02	-8.4	-0.01
	18	408.4 C	16.02	15.24	35.53	2.87	-	1.05	1.99	-47.2	-0.16
	19	409.00	17.20	15.40	36.35	2.46	-	4.08	5.40	-24.4	-0.06
	20	409.80	18.06	15.51	37.16	2.63	-	4.93	7.90	-37.6	-0.09
	21	411.75	16.83	15.41	36.24	2.83	-	2.51	4.35	-42.1	-0.12
Volcanics	22	414.36 i	18.96	15.59	37.07	1.89	-	10.65	10.52	1.2	0.00
	23	414.36 v	21.59	15.88	39.47	2.31	-	19.46	18.19	7.0	0.03
	24	417.45	19.74	15.66	37.56	1.90	-	14.40	12.81	12.4	0.03
	25	419.85	21.46	15.77	38.97	2.10	-	13.40	17.79	-24.7	-0.08
	26	422.70	20.72	15.79	38.54	2.13	-	14.50	15.64	-7.3	-0.02
	27	424.90	21.40	15.81	38.60	1.92	-	17.55	17.62	-0.4	0.00
	28	428.75	18.32	15.45	36.55	1.75	-	8.05	8.66	-7.0	-0.01
	29	431.40	20.15	15.63	37.91	1.97	-	14.62	13.99	4.5	0.01

Table 5.2: Measured major element oxides (weight percent) and trace element concentrations (ppm).

Oxides	Sediments											Upper Paleosol			
Wt.%	**398.85**	**400.35**	**401.3**	**401.4**	**402.3**	**403.9**	**404.1**	**404.75**	**405.1**	**405.2**	**405.7**	**406.4**	**406.7**	**406.4***	**407.2**
SiO_2	66.41	53.84	65.39	68.26	70.9	63.25	58.29	61.2	54.59	44.22	45.88	50.3	41.46	41.1	44.76
TiO_2	0.66	2.77	1.37	0.77	0.52	2.13	1.02	0.8	0.78	0.99	0.55	0.62	0.59	0.79	0.65
Al_2O_3	13.71	11.62	11.38	12.82	11.29	9.43	16.35	17.24	15.63	22.98	21.87	19.21	19.95	28.97	20.07
Fe_2O_3	7.65	19.89	11.32	7.99	8.87	15.37	11.4	7.5	15.47	13.49	12.95	12.19	18.31	9.5	16.14
MnO	0.08	0.09	0.1	0.09	0.12	0.14	0.13	0.09	0.16	0.18	0.19	0.21	0.31	0.13	0.2
MgO	2.02	1.75	1.99	1.84	2.24	2.05	1.87	1.67	2.49	2.96	2.76	2.71	5.45	2.34	3.51
CaO	0.68	0.83	1.14	1.13	1.43	2.05	2.23	1.47	1.38	1.09	2.57	4.75	1.79	0.83	2.32
Na_2O	0	0	0	0	0	0	0	0	0	0	0	0	0.22	0.07	0.02
K_2O	3.27	2.66	2.43	3.01	2.14	1.58	3.93	4.75	3.73	6.19	5.26	3.6	3.15	8.46	4.38
P_2O_5	0.15	0.15	0.12	0.09	0.1	0.11	0.15	0.13	0.16	0.27	0.18	0.14	0.13	0.11	0.15
Co_2	1.53	0.96	0.86	1.26	0.96	0.63	1.57	1.86	1.22	2.26	2.63	1.84	1.43	3.46	2
LOI	1.51	0.95	1.35	1.1	1.42	1.13	1.15	1.05	1.56	1.9	1.46	1.6	3.31	1.26	1.96
Total	**97.67**	**95.51**	**97.45**	**98.36**	**99.99**	**97.87**	**98.09**	**97.76**	**97.17**	**96.53**	**96.3**	**97.17**	**96.1**	**97.02**	**96.16**
CIA %	76	74	72	72	71	65	67	70	72	74	69	61	75	73	70
PIA %	92	88	83	84	79	69	77	84	85	92	79	65	83	94	80
U(ppm)	1.69	1.87	1.21	1.37	0.76	1.57	2.17	1.41	1.30	0.51	0.70	0.43	0.35	0.18	0.34
Pb(ppm)	2.86	2.90	3.24	3.46	2.96	3.45	5.22	3.05	2.51	1.44	5.41	6.79	3.37	1.88	3.47

*paleosol with thin oxidized layer, (C) Corestone of basalt, (P) Paleosol, (i) Layer of intrusion, (v) Volcanics.

Continuation of Table 5.2: Measured major element oxides (weight percent) and trace element concentrations (ppm).

Oxide	Upper Paleosol		Lower Paleosol				Volcanics							
Wt. %	**407.7**	**408.4 P**	**408.4 C**	**409.0**	**409.75**	**411.75**	**414.36 i**	**414.36 v**	**417.45**	**419.85**	**422.7**	**424.9**	**428.75**	**431.4**
SiO_2	39.78	53.46	60.24	52.66	48.03	58.03	48.6	49.35	53.46	42.74	49.18	48.95	48.42	51.73
TiO_2	0.69	0.48	0.45	0.51	0.55	0.39	0.51	0.48	0.52	0.54	0.59	0.5	0.57	0.4
Al_2O_3	23.35	19.43	15.79	18.1	18.14	15.85	18.82	15.75	17.67	17.46	17.31	15.93	16.02	13.66
Fe_2O_3	13.89	10.58	8.02	11.86	13.34	8.72	12.08	17.62	11.26	16.06	11.35	13.54	11.66	10.37
MnO	0.22	0.14	0.17	0.19	0.24	0.13	0.23	0.11	0.14	0.23	0.16	0.2	0.2	0.19
MgO	4.06	3.26	1.5	4.24	6.25	3.27	6.57	2.88	4.7	8.3	5.33	7.29	6.49	5.74
CaO	3.42	1.12	7.55	2.12	1.72	4.96	2.37	1.83	2.01	1.33	4.03	4.83	6.52	6.17
Na_2O	0	0	2.71	4.71	3.52	3.49	4.55	5.69	4.22	3.56	4.95	1.9	3.2	3.48
K_2O	5.09	5.01	0.3	0.41	0.38	0.1	0.14	0.03	1.04	0.07	0.05	0.08	0.39	0.3
P_2O_5	0.13	0.1	0.08	0.12	0.15	0.09	0.09	0.13	0.1	0.12	0.11	0.13	0.08	0.09
Co_2	2.73	2.4	0.8	0.96	1.2	0.89	1.22	0.64	1.1	2.78	2.27	1.43	2.23	3.35
LOI	2.27	1.65	0.93	1.99	2.92	1.42	2.81	0.95	1.9	3.27	2.09	2.89	2.54	1.95
Total	**95.63**	**97.63**	**98.54**	**97.87**	**96.44**	**97.34**	**97.99**	**95.46**	**98.12**	**96.46**	**97.42**	**97.67**	**98.32**	**97.43**
CIA %	67	73	46	61	67	52	62	56	61	68	53	58	48	44
PIA %	75	89	46	61	67	52	62	56	61	69	53	58	48	44
U(ppm)	0.39	0.15	0.18	0.18	0.15	0.17	0.25	0.36	0.23	0.25	0.24	0.43	0.18	0.24
Pb(ppm)	5.29	1.26	10.02	2.63	1.88	4.01	1.47	1.25	1.04	1.24	1.07	1.62	1.41	1.06

*paleosol with thin oxidized layer, (C) Corestone of basalt, (P) Paleosol, (i) Layer of intrusion, (v) Volcanics.

Table 5.3: Percentagegain/loss ratio for major and trace elements from altered samples relative to least altered sample. Constant TiO_2isconsidered through the profile, rather than constant mass or volume (Gresens, 1967). For sediments, the least altered sample is represented by the average upper crust composition (Taylor and McLennan, 1985). For paleosols,the least altered sample is represented by the average composition of the least two weathered volcanics. % gain/loss ratio $=\Delta C_i/C_i = [(C^o_{TiO2}/ C^A_{TiO2})(C^o_i/ C^A_i)-1]*100$ (Grant, 1986).For sediments, concentration of U in parent rock has been corrected by 1.89 ppm in average; a correction of 0 ppm was made for the least two weathered volcanic samples (see table 5.2).

Oxide	Sediments										
	398.85	**400.35**	**401.3**	**401.4**	**402.3**	**403.9**	**404.1**	**404.75**	**405.1**	**405.2**	**405.7**
CaO	-87	-96	-89	-81	-65	-88	-72	-77	-77	-86	-40
Na_2O	-100	-100	-100	-100	-100	-100	-100	-100	-100	-100	-100
K_2O	-16	-84	-70	-34	-30	-87	-35	1	-19	6	62
U	-71	-92	-90	-79	-83	-91	-75	-80	-81	-94	-85

Oxides	Upper Paleosol						Lower Paleosol			
	406.4	**406.7**	**406.41**	**407.2**	**407.7**	**408.4P**	**408.4C**	**409**	**409.8**	**411.75**
CaO	8	-57	-85	-50	-30	-67	137	-41	-56	80
Na_2O	-100	-95	-99	-100	-100	-100	-22	20	-17	17
K_2O	1036	945	1996	1219	1344	1943	30	57	35	-50
U	60	36	-48	19	29	-28	-9	-20	-38	-1

6 DISCUSSION

Whole-rock $^{206}Pb/^{204}Pb$ vs. $^{207}Pb/^{204}Pb$ isotope ratio diagram for volcanics (Figure 5.1) displays an almost linear array. Nonetheless, the age calculated (1906 ± 540 Ma), within uncertainty, agrees well with the radiometric age proposed to the system ~1.9 Ga (Stern et al., 1995). The almost linear arrangement of samples along the age slope in Figure 5.1 indicates that whole-rock samples' Pb isotopic composition of volcanics did not fractionate in the presence of green-schist metamorphism, as described by Holland et al. (1989); they were redistributed within the whole-rock.

The upper radiometric age range of sediments and paleosols (2040 and 2643 Ma, respectively) predates the age of the volcanics, thus such ages are meaningless. On the other hand, their lower age range (1800-1703 Ma, respectively) is concordant with the Hudsonian orogeny age range (2155-1750 Ma) (Stockwell, 1982). Therefore, the Hudsonian orogeny, a mountain-building event, exposed the volcanics to the atmosphere and instigated the formation of the paleosol and transportation of sediments after ~1.85 Ga(Pan and Stauffer, 2000, presents a maximum chemical age of 1.85 Ga for uraninite in the paleosols).

Although the $^{206/204}Pb$ vs. $^{207/204}Pb$ diagram for paleosol and sediments shows an almost linear array, indicative of close system behavior or loss of radiogenic Pb at constant rates, their ages are not concordant with the stratigraphic sequence they ought to follow. Calculated paleosols and sediments ages are older than the volcanics (base of the profile). By inspection of the $^{206/204}Pb$ vs. $^{207/204}Pb$ diagram, paleosol isotopic ratios are much lower than the volcanics, indicating the migration of radiogenic Pb out of the system in the paleosol zone or low accumulation of radiogenic Pb due to migration of U out of the system as volcanics were exposed to oxygenated weathering. On the other hand, sediments show radiogenic Pb ratios

greater than volcanics; either Pb was readily mobilized into the sediments or had more U available to decay into radiogenic Pb. Assuming that Pb behaves conservatively compared to U, then U mobility affected the true ages of palesols and sediments.

Time-integrated Th/U ($\kappa^{\dagger}$) vs. depth (Figure 5.2) shows variation in Th/U ratios, indicating that mass balance between the present radiogenic Pb and the present U concentration is not concordant, thus U was mobilized (gain and loss) in the paleosol and sediments. At the time of deposition, most of the radiogenic lead gained by sediments was uranogenic lead (indicated by horizontal variations in Figure 5.1), while subtle amounts of thorogenic lead were added to samples 1, 2, 8, and 9 relative to the Pb growth model for the upper crust model (Kramers and Tolstikhin, 1997). Sediments' time-integrated Th/U ($\kappa^{\dagger}$) ratio values range from 1.14 to 2.05 (1.59 in average) and is well below the κ=3.86 model, thus indicating U mineralization at the time of deposition or shortly after. Because Th is considered conservative in pedogenic profiles, κ changes correspond to a potential addition of U by 41% on average to the sediments, relative to average upper crust values at the time of deposition. Addition of U was likely possible by oxygenated fluids transporting uranyl ions and then precipitating with sediments as fluids became reduced, such as in the process of roll-front deposits (see discussion below).

Comparison between observed whole-rock ratios U/Pb (μ) and time-integrated U/Pb ($\mu^{\dagger}$) ratios in paleosols indicates that present U/Pb (μ)ratios are low to produce the amount of radiogenic Pb present in each sample (Table 5.1). Therefore, paleosols reveals losses of U up to 47% (corestone sample). The upper paleosol lost 12.8% average, and the lower paleosol lost 37.8% in average; such observation is confirmed by U-Pb isochron(Figure 5.8). U-Pb isochron shows a reference isochron at 1906 Ma. (average age for volcanics). Corestone sample (the least

weathered sample in the paleosol) lost most of the U, therefore a line passing through the lower paleosol samples would define the minimum U lost possible. It is evident that the upper paleosol samples (higher CIA values) lost less U than lower paleosols (lower CIA values), confirming an apparent addition of U to the upper paleosol or differential weathering between the upper and lower paleosol. A hypothesis for differential weathering is unlikely because upper paleosols were more exposed to oxidative weathering than lower paleosols, unless an oxigenated low groundwater table was present. But as seen below, the upper paleosol lost major oxides in a higher proportion than the lower paleosol.

The initial stages of high U enrichment at the time of deposition of sediments was likely initiated due to adsorption onto smectite clays, and also due to the inorganic reduction of uranyl (U^{+6}) to uranate (U^{+4}), as in the case of roll front/roll type deposits (Cheney and Tramell, 1973). Granger and Warren (1969) demonstrate the abiogenetic route of producing reducing conditions because of unstable sulfur compounds. In the volcanics, abundant pyrite is present; pyrite in contact with oxygenated fluids produces sulfates (SO_4^{2-}), bisulfate (HSO_3^-), and thiosulfates ($S_2O_3^-$) (Granger and Warren, 1969). Such reactions consume oxygen to create sulfates and release hydrogen ions (H^+), creating acidic conditions. Also, intermediate sulfur products may recombine with ferrous iron to form iron sulfide or reconstruct pyrite minerals, as experimentally demonstrated by Granger and Warren (1969). Therefore, reconstructed or previously present pyrite in the sediments in contact with oxygenated fluids would create reducing conditions enough to precipitate uranyl ions from fluids. Subsequent abundant flushing of oxygenated fluids would mobilize U from the sediments.

Extensive loss of Ca, K, and Na relative to average upper crust values is observed in the Missi sediments for present CIA values (65% to 76%, Figure 5.12). But, as seen in Figure 5.13,

pre-metasomatism CIA values for sediments reached maximum values ranging from 72% to 85%. Alkalis and alkaline earths, commonly found in plagioclase, are commonly reported to be lost in the pedogenic processes. Na and Ca are progressively removed as a function of increasing weathering intensity and K should also be removed at the same rate as Ca and Na; instead, K is the least removed ion. Conversion of plagioclase to smectite is common at high CIA values, as shown by the pre-metasomatism CIA values. As indicated by Figure 5.13, additions of K during post-metasomatism converted smectites to illites, due to the high affinity of large ions to exchange sites available in clays. Depletion of U in sediments relative to corrected value of U in the average upper crust (normalized to TiO_2, the least mobilized oxide within the profile) is observed as CIA values increase. Such depletion is expected under oxidative weathering given the geochemistry of U; $U^{+4}$is oxidized to U^{+6}. Similar leaching of alkalis and U was observed in 1.9 Ga sedimentary rocks from Northeastern Labrador, Canada under oxidizing conditions (Hayashi et al., 1997).

Removal of Ca and Na is observed in the paleosols during increasing weathering values (CIA 46%-75%). The least weathered sample in the lower paleosol shows an increment in Ca abundance relative to parent volcanics. As observed by Holland et al. (1989), epidote patches containing high amounts of Ca are present in the volcanics. Thus, weak weathering of basalts was not able to quickly leach out Ca from epidote as volcanics were transformed to paleosols. Similarly, two samples from the lower paleosol show an increase in Na content. In the volcanics, Na is mostly contained on albite, thus irregular mineralogy of the parent volcanics could explain such anomalies in Na distribution in the lower paleosol. K and U concentration trends show similar behavior in the lower and upper paleosol, but K and U concentrations are greater in the upper paleosol than in the lower paleosol, relative to parent volcanics. Thus parent volcanic

could not be the source of additional K and U in the paleosol, since paleosol concentrations are higher than in the parent volcanics. Instead, additional K and U could be correlated to basinal brines from overlaying sediments during post-metasomatism alteration (Figure 5.13).

U enrichment in the upper paleosol could be possible due to U adsorption onto clays and oxides or by precipitation of U due to reduction of basinal brines. Previous studies (Ames et al., 1982; Ames et al., 1983; Langmuir, 1978; Borovec, 1981) showed that clays themselves do not directly influence the accumulation of U. Also, as found in this study, K concentrations are higher in the oxidizing basinal brines, thus would compete for the sorption sites of smectites. On the other hand, higher U mineralization attributed to the reduction of basinal brines is reported in other paleosol studies (Fedo et al., 1996; Maynard, 1992; Hayashi et al., 1997).Therefore, U mineralization by the process of absorption onto smectites is unimportant compared to the reduction of basinal brines, and is reasonable that mineralization of U in the upper paleosol is associated with fluids coming from the overlying sediments.

The amount of U present in the profile is shown in Figure 6.1. The highest concentration is in the sediments (2.17 ppm, 1.32ppm in average). Though the sediments should be a good target for U recovery, its concentration is not cost-effective due to the low concentration compared to average upper crust values (2.8 ppm). But due to the loss of U from sediments, about 80% of U was lost relative to corrected U upper crust value, down-gradient structural traps with reducing fluids in the Missi sediments, overlying the upper paleosol, should be a good place for U mineralization.

Stauffer (1990) asserts that the Missi sediments are entirely composed of volcanic arc material (Amisk), although no geochemical evidence is presented. If that were the case, then Missi sediments would have mineralized U up to 500% relative to unaltered volcanics. Thus, a

geochemical provenance study for the Missi sediments is needed to determine the "true" extent of U mobility within the sediments.

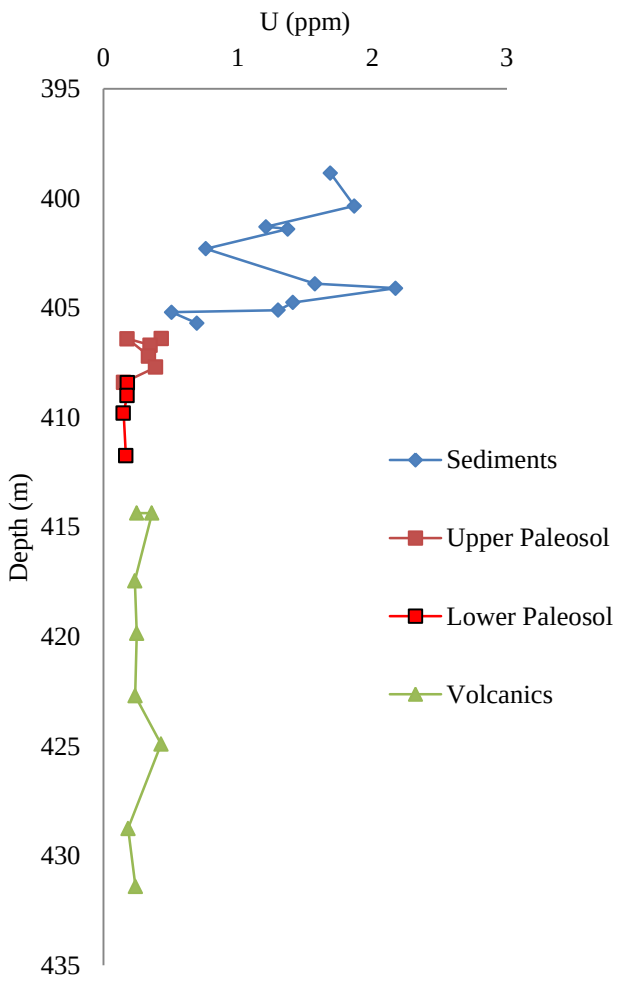

Figure 6.1 Measured uranium concentration (ppm) vs. depth.

7 CONCLUSIONS

A balance between Pb isotope ratios and the amount of U present in a rock helps to define a “True unaltered rock”; dissimilarity between the Pb isotope ratios and U content indicates post alteration. At the time of deposition, in the Missi sediments as much as ~58.9% of excess U was added to the sediments relative to Pb isotope model from Kramers and Tolstikhin (1997); while paleosol differences in U enrichment (upper paleosol, 25% higher than lower paleosol) are associated to metasomatism.

Noticed trends in chemical composition of major oxides for sediments from the Missi formation relative to average upper crust values present good agreement with their known geochemical behavior of labile and conservative major elements; with exception of K, which was added to the profile by post metasomatism. Such trends agree with previous studies in the same paleosol (Holland et. al., 1989, Pan and Stauffer, 2000).

Radiometric minimum ages of sediments and paleosols indicates the presence of a post-depositional event that altered the geochemistry of the parent basalt. These ages are bracketed by the most important folding event in the Churchill province, the Trans-Hudson orogeny (2155 – 1750 Ma) (Stockwell, 1982), which resulted in the alteration of κ and μ ratios by exposing volcanics to the atmosphere and instigating the mobilization of U due to its redox sensitive behavior.

Currently, in the Missi sediments U have been lost by 84% average relative to corrected average upper crust value; in the upper paleosol U have been gained by 11% and the lower paleosol lost U by 17%, relative to least weathered parent volcanics. Such difference in U mobility in the paleosol indicates potential mineralization of uranium at the unconformity between Missi sediments and paleosol or down-gradient at structural or unconformity

trapscontaining rocks that can help reduce oxygenated fluids (i.e. shale rocks). Even though U variation between parent and altered rock is not economically important, accumulation over geologic times may constitute a major source of uranium.

REFERENCES

Ames, L.L., McGarrah, J.E., Walker, B.A., Salter, P.F., 1982. Sorption of uranium and cesium by Hanford basalts and an associated secondary smectite. Chemical Geology. v.35,205-225.

Ames L.L., Mc-Garrah J.E., Walker B.A. and Salter P.F., 1983. Uranium and Radium sorption on amorphous ferric oxyhydroxide. Chemical Geology, v.40, 135-148.

Borovec, Z., 1981. The adsorption of uranyl species by fine clay. Chemical Geology, v.32, 45-58.

Best, M.G., 1982.Igneous and methamorphic petrology. New York: W.H. Freeman; see Chapter 3.

Cheney, E. S., and Trammell, J. W., 1973. Isotopic evidence for inorganic precipitation of uranium roll ore bodies. American Association of Petroleum Geologists Bulletin,v.57,1297-1304.

Dickie, J. M., 2010. Mineralogical and Geochemical Indicators of Subaerial Weathering in the Pozzolane Rosse Ignimbrite (AlbanHills Volcanic District, Italy). Geosciences Theses. Paper 23. http://digitalarchive.gsu.edu/geosciences_theses/23

Doe, B.R., Stuckless, J.S., Delevaux, M.H., 1983. The possible bearing of the granite of the UPH deep drill holes, northern Illinois, on the origin of Mississippi Valley ore deposits. Journal of Geophysical Research, v.88, 7335-7345.

Faure, G. and Mensing, T.M. (2005). Isotopes: Principles and Applications. John Wiley& Sons.897 pp.

Fedo, C.M., Nesbitt, H.W. and Young, G.M. 1995. Unraveling the effects of potassium metasomatism in sedimentary rocks and paleosols, with implications for paleoweathering conditions and provenance. Geology,v.23, 921-924.

Fedo, C.M., Eriksson, K.A. and Krogstad, E.J., 1996. Geochemistry of shales from the ~3.0 Ga Buhwa Greenstone Belt, Zimbabwe: implications for provenance and source-area weathering. Geochimica CosmochimicaActa, v.60, 1751-1763.

Galley, A.G., Syme, E.C., and Bailes, A.H., 2007.Mineral Deposits of Canada: A Synthesis of Major Deposit Types, District Metallogeny, the Evolution of Geological Provinces, and Exploration Methods: Geological Association of Canada, Mineral Deposits Division, Special Publication No. 5, p. 509-531

Granger, H.C. and Warren, C.G., 1969. Unstable sulfur compounds and the origin of roll-type uranium deposits. Economic Geology, v. 64, 160-171.

Grant, J.A., 1986. The isocon diagram-a simple solution to Gresens' equation for metasomatic alteration. Economic Geology,v. 81,1976-1982.

Grant, J.A., 2005. Isocon analysis: a brief review of the method and applications. Physics and Chemistry of the Earth,v. 30, 997–1004.

Gresens, R.L., 1967. Composition-volume relationship of metasomatism. Chemical Geology,v. 2, 47-54.

Hayashi, K., Fujisawa, H., Holland, H.D. and Ohmoto, H., 1997. Geochemistry of 1.9 Ga Sedimentary Rocks from Northeastern Labrador, Canada. Geochimica Cosmochimica Acta, v.19, 4115-4137.

Heiri O., Lotter A. F., Lemcke G., 2001.Loss on ignition as a method for estimating organic and carbonate content in sediments: reproducibility and comparability of results. Journal of Paleolimnology,v.25, 101–110.

Holland, H.D., Feakes, C.R., and Zbinden, E.A., 1989. The Flin Flon paleosol and the composition of the atmosphere 1.8 BYBP. American Journal of Science, v.4, 362-389.

Kay, R. W., 1977 In Island arcs, deep sea trenches, and back-arc basins (ed. M. Talwani & W. Pitman) (Maurice Ewing Series, 1), 229-242. Washington, D.C.: American Geophysical Union.

Kramers, J.D., Tolstikhin, I.N., 1997. Two terrestrial lead isotope paradoxes, forward transport modelling, core formation and the history of the continental crust. Chemical Geology, v.139, 75-110.

Krogstad, E.J., Walker, R.J., Nabelek, P.I. and Russ-Nabelek, C., 1993. Pb isotopic evidence for mixed sources for Proterozoic granites and pegmatites, Black Hills, South Dakota, USA. Geochimica Cosmochimica Acta, v.57, 4677-4685.

Krogstad, E.J. and Walker, R.J., 1996. Evidence of heterogeneous crustal sources: the Harney Peak Granite, South Dakota, U.S.A. Transactions of the Royal Society of Edinburgh: Earth Sciences, v.87, 331-337.

Krogstad, E.J., 2004. The Pb isotope records of Archean and Proterozoic shales limit early O-rich atmosphere. Eos, Transactions, American Geophysical Union, 85.

LaTour, T.E., 1989. Analysis of rocks using X-ray fluorescence spectrometry. Rigaku Journal, issue 6, 3-9.

Langmuir, D., 1978. Uranium solution-mineral equilibria at low temperatures with applications to sedimentary ore deposits. Geochimica et CosmochimicaActa, v. 42, 547–569.

Lucas, S.B., Stern, R.A., Syme, E.C., Reilly, B.A., and Thomas, D.J., 1996. Intraoceanic tectonics and the development of continental crust: 1.92-1.84 Ga evolution of the Flin Flon Belt, Canada; Geologic Society of America Bulletin, v.108,602-629.

Ludwig, K.R., 2001, Isoplot 3.0-A geochronological toolkit for Microsoft Excel: Special publication No. 4, Berkeley Geochronology Center, Berkeley, Calif., 71 p

Maynard, J. B., 1992. Chemistry of modern soils as a guide to interpreting Precambrian paleosols: Journal of Geology, v.100, 279–289.

McLennan, S.M., Taylor, S.R., 1980. Th and U in sedimentary rocks: crustal evolution andsedimentary cycling. Nature, v. 285, 621–624.

Nesbitt H.W., 1979. Mobility and fractionation of rare earth elements during weathering of a granodiorite. Nature, v.279, 206-210.

Nesbitt, H.W. and Young, G.M., 1984. Prediction of some weathering trends of plutonic and volcanic rocks based on thermodynamic and kinetic considerations. Geochim.Cosmochim.Acta, v.48, 1523-1534

Pan,Y. and Stauffer, M. R., 2000. Cerium anomaly and Th/U fractionation in the 1.85 Ga Flin Flon Paleosol; clues from REE- and U-rich accessory minerals and implications for paleoatmospheric reconstruction. American Mineralogist, v.85, 898-911

Pollack, G.D., Krogstad, E.J., Bekker, A., 2009, U-Th-Pb-REE systematics of organic-rich hales from the ca. 2.15 Ga Sengoma Argillite Formation, Botswana: Evidence for oxidative continental weathering during the Great Oxidation Event, Chemical Geology, v. 260, 172-185.

Rehkämper, M., Mezger, K., 2000. Investigation of matrix effects for Pb isotope ratio measurements by multiple collector ICP-MS: verification and application of optimized analytical protocols. Journal of Analytical Atomic Spectrometry, v.15, 1451–1460.

Rosholt, J.N., and Bartel, A.J., 1969. Uranium, Thorium and lead systematics in Granite Mountains, Wyoming: Earth and Planetary Science Letters, v. 7, 141-147.

Rosholt, J.N., Zartman, R.E., Nkomo, I. T., 1973. Lead Isotope systematics and uranium depletion in the Granite Mountains Wyoming. The Geological Society of America Bulletin, v. 84; no.3, 989-1002.

Rye, R., Holland, H.D., 1998. Paleosols and the evolution of atmospheric oxygen: A critical review. American Journal of Science, v. 298, 621-672.

Schulz, K.J., Cannon, W.F., 2007.The Penokean orogeny in the Lake Superior regions. Precambrian Research, v.157, 4-25.

Sicree, A.A., Barnes H.L., 1996. Upper Mississippi Valley district ore fluid model: the role of organic complexes. Ore Geology Reviews, v.11, 105-131

Stauffer M. R., 1990. The Missi Formation: an Aphebian Molasse deposit in the Reindeer Lake zone of the Trans-Hudson Orogen, Canada, in Lewry, J.F. and Stauffer, M.R., eds., The Early Proterozoic Trans-Hudson of North America: Geological Association of Canada, Special Paper 37, 121-141.

Stern, R. A., Syme, E. C., Bailes, A. H., and Lucas, S. B., 1995. Paleoproterozoic (1.90 –1.86 Ga) arc volcanism in the Flin Flon Belt,Trans-Hudson Orogen, Canada: Contributions to Mineralogy and Petrology, v.119, 117–141.

Stockwell, C. H., 1982. Proposals for time classification and correlation of Precambrian rocks and events in Canada and adjacent areas of the Canadian shield. Part 1: A time classification of Precambrian rocks and events. Geological Survey of Canada Paper 80–19, 135 pp. +4 folding maps and two folding histogram sheets with Figures 10, 11 and 17.

Sun, S. S., 1980. Lead isotopic study of young volcanic rocks from mid- ocean ridges, ocean islands and island arcs. Phil. Trans. Royal Society of London. A 297, 409 45.

Taylor, S. R. and McLennan, S. H., 1985. The Continental Crust: Its Composition and Evolution. Blackwell, Oxford, 312 pp.

Thorpe, R.I., 2008. Release of lead isotope data in 4 databases: Canadian, Western Superior, foreign, and whole rock and feldspar, Geological Survey of Canada, OF 5664.

White, W.M., 1993. U-238/Pb-204 in MORB and open system evolution of the depleted mantle. Earth and Planetary Science Letters, v. 115, 211-226.

APPENDICES

APPENDIX 1: Pb Isotope Analytical Methodology

Whole-rock digestion procedure

Digestions were made under class-100 laminar flow hoods, with the purpose of reducing contamination from airborne particulate matter. All digestions used 7 mL PFA Teflon® Savillex vials. Initially, vials were cleaned using a solution of Citranox® liquid acid cleanser and tap water; rinsed with deionized water and placed in a 10% trace metal grade nitric acid bath overnight; next, vials were taken out of bath and rinsed with MilliQ® water, making sure extraneous material were not attached to vial interior walls; then, 1 mL of 2 M Trace Metal grade acid nitric was added to each vial, capped and placed on a hot plate overnight; lastly, vials were removed from the hotplate, acid was discarded, and vials were rinsed with MilliQ® water.

The digestion technique used was based in the procedures suggested by Krogstad and Walker (1996). Upon cleaning vials; vials were labeled a minimum of 100 mg of powder sample was added to vials; three drops of ^{205}Pb-^{235}U whole-rock spike were added to each vial; then, vials were carried to hot plate where 10 drops of Optima® Nitric acid (15.6M) and 40drops of Optima® Hydrofluoric acid (28.9M) were added to each vial; vials were capped for overnight digestion; next day, vials were dried and added 10 drops of HNO_3 and 40 drops of HF, this last step was repeated to ensure maximum dissolution of silicates contained in rock powder. Finally, after drying digested sample, 6 mL of 2M Optima® HCL was added to vial, vilas were capped and placed under laminar flow hood with the purpose of letting particulate settle in the bottom of vials.

Column chemistry procedure

Pb is separated using AG1-8x anion resin in Teflon columns. Teflon columns were made using 4:1 PTFE Heat Shrinkable Teflon® tubing, with 3:1 volumetric dimensions. Resin in a 2M HCL was pipetted onto the column until ¼ volume of the column was filled with resin; then, MilliQ® water was added assuring no obstructing bubbles were present in the column, this last step was achieved by squeezing back and forth MilliQ® water onto the column aided with a transfer. To clean up these columns, the following acids and water were allowed to run through the column; one reservoir volume of 6M HCl Optima® grade acid; followed by one reservoir volume of MilliQ® water; and ½ reservoir of HBr Optima® grade acid, this step was necessary to adjust the resin to a bromide form, which will allow lead bromide complexes to be retained in the column.

Chemical separation of lead and uranium was carried following the steps suggested by Krogstad et al. (1993) and Krogstad et at. (1996). Once the anion resin exchange columns were cleaned, they were ready for the introduction of the sample fluid (2M Optima® HCl with dissolved ions from digested sample). First; a clean 7mL vial is placed under column to collect 3mL of sample fluid transmitted through resin, a pipette cleaned with a 2M HNO_3 acid trace metal grade was used to transfer sample liquid from vial to column; once column was empty of liquids, add 1 reservoir volume of 0.5M Optima® HBr acid to column, this step washes specific cations such as transition metals remove; after HBr acid goes through, a half reservoir of 2M Optima® HCl acid is added to column, this step remove cations such as alkali metals ions such as K and Na that were not previously removed; after HCl run though resin, 7mL vial container that collected all previously liquids transmitted through column is placed on the hot plate uncapped to dry down all liquids, the dry down material left is termed “goop”. Finally, a 7mL

clean vial is placed under column; Lead is eluted from column by adding one reservoir volume of 6M Optima® HCl, this step dissolves lead that was attached to resin in column; after HCl goes through column, 2 drops of Optima® Nitric acid (15.6M) are added to vial; vial containing eluted lead is placed to hot plate at 120 ^{o}C to dry; then, 2 more drops of Optima® Nitric acid (15.6M) is added and let the vial dry down liquids, this step is repeated twice; lastly after all liquids are dried down, 1.5 mL of MilliQ® water is added to vial to allow lead be in solution, this solution is used for mass spectrometry analysis.

For the chemical separation of uranium, columns have to be washed by letting run through them one reservoir volume of MilliQ® water, then 1 reservoir volume of 7M Optima® HNO_3, columns will be ready for "goop" in solution. Once columns are washed, a waste container is placed under columns; "goop" in solution is completely loaded onto columns; after column is empty of liquids, a reservoir of 7M Optima® HNO_3 is added, this step washes away all cations from column leaving only Uranium and Thorium attached to resin. Then after all liquids have run through the column, uranium is eluted from the column into a clean vial by adding one reservoir of MilliQ® water to the column. Finally, vial containing eluted uranium is placed on a hot plate at 120 ^{o}C to dry down liquids, a gray to reddish bead (spec size) should be left; then, 2 drops of Optima® Nitric acid (15.6M) are added to vial and let vial dry down, this last step is repeated twice. Finally, 1.5 mL of MilliQ® water is added to vial, so uranium is in solution ready for mass spectrometry analysis.

APPENDIX 2: XRF Analytical Methodology

XRF procedure

The analysis followed the methodology outlined by La Tour (1989). To make fused disc; first, 0.5 gr of powdered sample was mixed with 4.5 gr of lithium tetraborate. Then, the mixture is fused in a 95%Pt- 5%Au and placed in a furnace at approximately 1150°C for 15 minutes, stirring is necessary to form a homogeneous melt. Finally, the homogeneous melt is poured into a preheated mold to chill to form a thick glass disc, this step is done onto a torch flame, glass disc is placed into a desiccating jar to cool down at room temperature for a minimum of 24 hours.

Previous to running glass discs, element interference of minerals with different composition will cause absorption/enhancement of fluorescence radiation or spectral overlap caused by neighboring elements in the periodic table, which could lead to large analytical error detected by the XRF spectrometer (La Tour, 1989); therefore, a reference disc is analyzed first for “alpha correction” to ensure a linear calibration curve. Fortunately, the Rigaku 3270 system will perform calculations to correct for overlap and matrix effects (La Tour, 1989). Analyte intensities measured by the spectrometer are automatically reduced to oxide concentrations using the fundamental parameters of the software package used by the instrument.

Loss on Ignition was calculated following the method of Heiri et. al (2001). Volatiles such as water, organic matter, and carbonate content may be estimated by weight loss measurements, in samples subjected to sequential heating. Water content in samples was estimated by drying samples at 60°C for 36 hours, water loss is accurately estimated as the weight percent difference between sample pre- and post- drying. Organic matter is combusted in a first step to ash and carbon dioxide at a temperature between of 550 °C, organic matter is

calculated as the difference in weight percent between samples dried at 60°C and the ash created following ignition at 550°C.

Appendix 3: Error estimates for ICPMS Measurements. Precision was calculated from repetitive measurements (n=6) of references SRM982 and SRM981. Accuracy was calculated using reference SRM982 (NIST) and accepted reference values.

	SRM981 Linearly Corrected to SRM982			**SRM981 Accepted Reference Values**		
# of Runs	**206Pb/204Pb**	**207Pb/204Pb**	**208Pb/204Pb**	**206Pb/204Pb**	**207Pb/204Pb**	**208Pb/204Pb**
1	17.0023	15.5743	36.9094	16.9371	15.4913	36.7213
2	16.9708	15.5420	36.8190	16.9371	15.4913	36.7213
3	17.0301	15.5725	36.9051	16.9371	15.4913	36.7213
4	16.9548	15.5375	36.7588	16.9371	15.4913	36.7213
5	17.0032	15.5445	36.8520	16.9371	15.4913	36.7213
6	17.0019	15.5569	36.8814	16.9371	15.4913	36.7213
2*std	0.0032	0.0021	0.0032			
Precision%	**0.32**	**0.21**	**0.32**			
Accuracy%	**100.00**	**100.00**	**100.00**			

Appendix 4: Error estimates for XRF Measurements. Precision was calculated from repetitive measurements (n=10) of sample 431.4 (volcanic) from this study. Accuracy was calculated using reference glass-disk BHVO-1 (USGS) and using accepted reference values.

Oxides	Sample 431.4 (Volcanic)												
Wt.%	1	2	3	4	5	6	7	8	9	10	Average	STV. DEV	Precision %
SiO_2	51.84	51.42	51.67	51.72	51.7	51.66	51.66	51.7	51.7	51.69	51.68	0.21	0.803
TiO_2	0.4	0.4	0.4	0.4	0.4	0.4	0.4	0.4	0.4	0.4	0.40	0.00	0.000
Al_2O_3	13.76	13.72	13.66	13.73	13.77	13.68	13.69	13.7	13.64	13.69	13.70	0.08	1.209
Fe_2O_3	10.49	10.53	10.49	10.47	10.49	10.45	10.48	10.45	10.45	10.51	10.48	0.05	1.025
MnO	0.19	0.19	0.19	0.19	0.19	0.19	0.19	0.19	0.19	0.19	0.19	0.00	0.000
MgO	5.83	5.82	5.79	5.82	5.77	5.78	5.81	5.76	5.78	5.75	5.79	0.06	1.911
CaO	6.21	6.17	6.17	6.18	6.18	6.17	6.18	6.18	6.18	6.18	6.18	0.02	0.747
Na_2O	3.57	3.58	3.6	3.57	3.55	3.49	3.53	3.53	3.5	3.52	3.54	0.07	4.059
K_2O	0.31	0.31	0.3	0.3	0.3	0.31	0.3	0.3	0.3	0.3	0.30	0.01	6.377
P_2O_5	0.09	0.09	0.09	0.09	0.09	0.09	0.09	0.09	0.09	0.09	0.09	0.00	0.000

Oxide	Number of Analyses on BHVO-1 Reference Glass Disk													
Wt.%	1	2	3	4	5	6	7	8	9	10	11	Average	BHVO-1 Ref. Val.	Accuracy %
SiO2	50.71	50.91	51	50.95	51.03	51.1	51.04	51.1	51.11	51.09	51.19	51.02	49.94	99.98
TiO2	2.79	2.78	2.8	2.8	2.79	2.8	2.8	2.78	2.81	2.8	2.8	2.80	2.71	99.97
Al2O3	14.04	14.05	14.05	14.04	14.07	14.08	14.06	14.04	14.06	14.06	14.05	14.05	13.80	99.98
Fe2O3	12.46	12.3	12.33	12.57	12.48	12.41	12.54	12.53	12.5	12.52	12.59	12.48	12.23	99.98
MnO	0.18	0.18	0.18	0.18	0.18	0.18	0.18	0.18	0.18	0.18	0.18	0.18	0.17	99.94
MgO	7.83	7.91	7.86	7.94	7.8	7.85	8.00	7.86	7.87	7.86	7.83	7.87	7.23	99.91
CaO	11.62	11.69	11.69	11.74	11.72	11.72	11.8	11.84	11.89	11.91	11.9	11.77	11.40	99.97
Na2O	3.81	3.83	3.83	3.87	3.82	3.86	3.86	3.77	3.86	3.78	3.72	3.82	2.26	99.31
K2O	0.63	0.63	0.63	0.63	0.63	0.63	0.63	0.64	0.63	0.63	0.63	0.63	0.52	99.79
P2O5	0.41	0.42	0.41	0.42	0.42	0.42	0.42	0.42	0.42	0.42	0.42	0.42	0.27	99.45